

- [18] Pelletier CC, Koppe L, Croze ML, Kalbacher E, Vella RE, Guebre-Egziabher F, et al. White adipose tissue overproduces the lipid-mobilizing factor zinc alpha2-glycoprotein in chronic kidney disease. *Kidney Int* 2013;83:878–86.
- [19] Schober A, Knarren S, Lietz M, Lin EA, Weber C. Crucial role of stromal cell-derived factor-1alpha in neointima formation after vascular injury in apolipoprotein E-deficient mice. *Circulation* 2003;108:2491–7.
- [20] Moreno Junior H, Nathan LP, Metzke K, Costa SK, Antunes E, Hyslop S, et al. Non-specific inhibitors of nitric oxide synthase cause myocardial necrosis in the rat. *Clin Exp Pharmacol Physiol* 1997;24:349–52.
- [21] Ono Y, Ono H, Matsuoka H, Fujimori T, Frohlich ED. Apoptosis, coronary arterial remodeling, and myocardial infarction after nitric oxide inhibition in SHR. *Hypertension* 1999;34:609–16.
- [22] Verhagen AM, Hohbach J, Joles JA, Braam B, Boer P, Koomans HA, et al. Unchanged cardiac angiotensin II levels accompany losartan-sensitive cardiac injury due to nitric oxide synthase inhibition. *Eur J Pharmacol* 2000;400:239–47.
- [23] Ikeda K, Nara Y, Tagami M, Yamori Y. Nitric oxide deficiency induces myocardial infarction in hypercholesterolaemic stroke-prone spontaneously hypertensive rats. *Clin Exp Pharmacol Physiol* 1997;24:344–8.
- [24] Suda O, Tsutsui M, Morishita T, Tanimoto A, Horiuchi M, Tasaki H, et al. Long-term treatment with N(omega)-nitro-L-arginine methyl ester causes arteriosclerotic coronary lesions in endothelial nitric oxide synthase-deficient mice. *Circulation* 2002;106:1729–35.
- [25] Braun A, Trigatti BL, Post MJ, Sato K, Simons M, Edelberg JM, et al. Loss of SR-BI expression leads to the early onset of occlusive atherosclerotic coronary artery disease, spontaneous myocardial infarctions, severe cardiac dysfunction, and premature death in apolipoprotein E-deficient mice. *Circ Res* 2002;90:270–6.
- [26] Zhang S, Picard MH, Vasile E, Zhu Y, Raffai RL, Weisgraber KH, et al. Diet-induced occlusive coronary atherosclerosis, myocardial infarction, cardiac dysfunction, and premature death in scavenger receptor class B type I-deficient, hypomorphic apolipoprotein ER61 mice. *Circulation* 2005;111:3457–64.
- [27] Nakagawa-Toyama Y, Zhang S, Krieger M. Dietary manipulation and social isolation alter disease progression in a murine model of coronary heart disease. *PLoS One* 2012;7:e47965.
- [28] Taddei S, Virdis A, Ghiadoni L, Magagna A, Favilla S, Pompella A, et al. Restoration of nitric oxide availability after calcium antagonist treatment in essential hypertension. *Hypertension* 2001;37:943–8.
- [29] Tsuji H, Venditti Jr FJ, Manders ES, Evans JC, Larson MG, Feldman CL, et al. Reduced heart rate variability and mortality risk in an elderly cohort. The Framingham Heart Study. *Circulation* 1994;90:878–83.
- [30] Baylis C. Nitric oxide deficiency in chronic kidney disease. *Am J Physiol Renal Physiol* 2008;294:F1–9.
- [31] Schmidt RJ, Baylis C. Total nitric oxide production is low in patients with chronic renal disease. *Kidney Int* 2000;58:1261–6.
- [32] Wever R, Boer P, Hijmering M, Stroes E, Verhaar M, Kastelein J, et al. Nitric oxide production is reduced in patients with chronic renal failure. *Arterioscler Thromb Vasc Biol* 1999;19:1168–72.
- [33] Lu TM, Chung MY, Lin CC, Hsu CP, Lin SJ. Asymmetric dimethylarginine and clinical outcomes in chronic kidney disease. *Clin J Am Soc Nephrol* 2011;6:1566–72.
- [34] Piatti P, Di Mario C, Monti LD, Fragasso G, Sgura F, Caumo A, et al. Association of insulin resistance, hyperleptinemia, and impaired nitric oxide release with in-stent restenosis in patients undergoing coronary stenting. *Circulation* 2003;108:2074–81.
- [35] Cooke JP. ADMA: its role in vascular disease. *Vasc Med* 2005;10(Suppl. 1):S11–7.
- [36] Cook S. Coronary artery disease, nitric oxide and oxidative stress: the “Yin-Yang” effect, a Chinese concept for a worldwide pandemic. *Swiss Med Wkly* 2006;136:103–13.
- [37] Shamseddin MK, Parfrey PS. Sudden cardiac death in chronic kidney disease: epidemiology and prevention. *Nat Rev Nephrol* 2011;7:145–54.
- [38] Sata M, Saiura A, Kunisato A, Tojo A, Okada S, Tokuhisa T, et al. Hematopoietic stem cells differentiate into vascular cells that participate in the pathogenesis of atherosclerosis. *Nat Med* 2002;8:403–9.
- [39] Shimizu K, Sugiyama S, Aikawa M, Fukumoto Y, Rabkin E, Libby P, et al. Host bone-marrow cells are a source of donor intimal smooth-muscle-like cells in murine aortic transplant arteriopathy. *Nat Med* 2001;7:738–41.
- [40] Ceradini DJ, Kulkarni AR, Callaghan MJ, Tepper OM, Bastidas N, Kleinman ME, et al. Progenitor cell trafficking is regulated by hypoxic gradients through HIF-1 induction of SDF-1. *Nat Med* 2004;10:858–64.
- [41] Zhang LN, Wilson DW, da Cunha V, Sullivan ME, Vergona R, Rutledge JC, et al. Endothelial NO synthase deficiency promotes smooth muscle progenitor cells in association with upregulation of stromal cell-derived factor-1alpha in a mouse model of carotid artery ligation. *Arterioscler Thromb Vasc Biol* 2006;26:765–72.
- [42] Mason RP, Walter MF, Trumbore MW, Olmstead Jr EG, Mason PE. Membrane antioxidant effects of the charged dihydropyridine calcium antagonist amlodipine. *J Mol Cell Cardiol* 1999;31:275–81.



Usefulness of the apparent diffusion coefficient (ADC) for predicting the consistency of intracranial meningiomas



Akira Yogi ^{a,*}, Tomomi Koga ^a, Kimei Azama ^a, Daichi Higa ^a, Kazuhiko Ogawa ^{a,b}, Takashi Watanabe ^c, Shogo Ishiuchi ^c, Sadayuki Murayama ^a

^a Department of Radiology, Graduated School of Medical Science, University of the Ryukyus, Okinawa, Japan

^b Department of Radiation Oncology, Osaka University Graduate School of Medicine, Osaka, Japan

^c Neurosurgery, Graduated School of Medical Science, University of the Ryukyus, Okinawa, Japan

ARTICLE INFO

Article history:

Received 27 December 2013

Received in revised form 4 June 2014

Accepted 24 June 2014

Keywords:

Meningioma

Consistency

DWI

ADC

ABSTRACT

Meningioma consistency is an important factor for surgical treatment. Tumor cellularity and fibrous tissue contribute to the consistency of tumors, and it is proposed that the minimum apparent diffusion coefficient (ADC) value is significantly correlated with meningioma consistency. Twenty-seven consecutive patients with 28 meningiomas were retrospectively enrolled. Minimum ADC values in meningiomas with a hard consistency were significantly lower than those with a soft consistency. The minimum ADC value might have clinical use as a predictor of meningioma consistency.

© 2014 Elsevier Inc. All rights reserved.

1. Introduction

Meningiomas are one of the most common intracranial benign neoplasms in adults; they arise from meningotheial cells of the arachnoid layer. The incidence of meningiomas has been increasing [1–3], in part due to technological advancement of radiologic imaging in the ability to detect small meningiomas [1,3,4]. Typical meningiomas are seen as a sharply circumscribed isodense masses that are isodense to cortex on computed tomography (CT) images. On magnetic resonance imaging (MRI), a meningiomas are often isointense or slightly hypointense on T1-weighted images (T1WI), and variably hypointense to hyperintense on T2-weighted images (T2WI). This variability of signal change depends on the amount of tumor calcification, fibrous tissue, necrosis, vascularity, and histological cell types [5]. Marked and relatively homogeneous contrast enhancement with a dural tail sign is also typically seen.

Surgical resection is often the treatment of choice for symptomatic meningiomas. The consistency of meningiomas is an important factor in developing the strategy of surgical resection and predicting the degree of removal; soft tumors are easily curetted by suctioning, whereas hard tumors frequently require a lengthy and tedious dissection. A noninvasive technique that enables surgeons to preoperatively assess the mechanical properties of meningiomas

could provide valuable information affecting risk assessment, patient management, and workflow optimization. In the case of hard meningiomas, preoperative transarterial embolization is a useful method to soften tumors and facilitate resection, especially when they are located at a complex site such as cavernous sinus, clivus, cerebellopontine angle, and sellar lesion [4,6]. Though some investigators have employed T1WI and T2WI for this purpose, it remains inaccurate because amount of water is not the only factor affecting tumor consistency [6–9].

Diffusion weighted image (DWI) and the apparent coefficient (ADC) map, derived from DWI, can provide information of water diffusion. Some studies in glioma suggest that ADC value has a strong correlation with tumor cellularity, and therefore it also strongly correlates with World Health Organization (WHO) grade, treatment effect, and prognosis [9,10,13–15]. Furthermore, it has been reported that the ADC value also correlates with the amount of fibrous tissue [16,17]. Both tumor cellularity and the amount of fibrous tissue contribute the consistency of tumors, and it is supposed that the intratumoral ADC value has a significant correlation with the consistency of meningiomas. Nevertheless, to our knowledge, there have been no reports regarding the relationship between the quantitatively measured ADC value and the consistency of meningiomas. Although some studies reported the usefulness of diffusion tensor imaging and MR elastography to predict the consistency of tumor [18–23], these advanced MR techniques require special equipment and software, and are not still commonly used in clinical purpose. In contrast, DWI is now commonly accepted as a part of conventional MR examination in most institutes. For these reason, it is

* Corresponding author. Department of Radiology, Graduate School of Medical Science, University of the Ryukyus, 207 Uehara, Nishihara-cho, Nakagami-gun Okinawa, 903–0215, Japan. Tel.: +81 98 895 1162; fax: +81 98 895 1420.

E-mail address: jxo98ayg@med.u-ryukyu.ac.jp (A. Yogi).

Table 1
Summary of cases

Case	Location	Histologic subtypes	ADC _{min} ($\times 10^{-3}$ mm ² /s)	ADC _{max} ($\times 10^{-3}$ mm ² /s)	ADC _{mean} ($\times 10^{-3}$ mm ² /s)	Consistency
1	CPA	Psammomatous	0.477	1.470	0.796	Hard
2	CPA	Fibroblastic	0.451	3.530	0.865	Hard
3	Sphenoid ridge	Meningothelial	0.519	1.283	0.814	Hard
4	Convexity	Meningothelial	0.595	1.286	1.812	Hard
5	Petroclival	Meningothelial	0.584	2.402	1.128	Hard
6	Convexity	Angiomatous	0.633	1.957	0.977	Hard
7	Convexity	Fibroblastic	0.253	1.162	0.892	Hard
8	Petroclival	Meningothelial	0.702	1.978	1.133	Hard
9	Convexity	Transitional	0.449	2.235	0.832	Hard
10	Convexity	Meningothelial	0.560	1.635	0.936	Hard
11	Tuberculum sellae	Meningothelial	0.109	2.129	0.877	Hard
12	Parasagittal	Transitional	0.615	1.771	0.850	Hard
13	Sphenoid ridge	Secretory	0.553	2.342	1.233	Hard
14	CPA	Meningothelial	0.465	2.861	1.330	Hard
15	Sphenoid ridge	Meningothelial	0.582	1.298	0.834	Hard
16	Sphenoid ridge	Meningothelial	0.684	2.337	1.034	Hard
17	Parasagittal	Meningothelial	0.628	1.692	0.769	Hard
18	Sphenoid ridge	Atypical	0.538	3.038	0.885	Soft
19	Sphenoid ridge	Angiomatous	0.802	2.863	1.521	Soft
20	CPA	Fibroblastic	0.597	2.036	0.905	Soft
21	Sphenoid ridge	Transitional	0.729	2.589	0.958	Soft
22	Parasagittal	Angiomatous	0.666	2.395	1.314	Soft
23	Sphenoid ridge	Meningothelial	0.638	1.136	0.830	Soft
24	Tuberculum sellae	Angiomatous	0.950	2.945	1.179	Soft
25	Parasagittal	Meningothelial	0.736	1.507	0.982	Soft
26	CPA	Transitional	0.741	1.076	0.872	Soft
27	Tuberculum sellae	Meningothelial	0.815	1.717	1.065	Soft
28	CPA	Meningothelial	1.488	2.108	1.708	Soft

ADC_{min}: minimum ADC.ADC_{max}: maximum ADC.ADC_{mean}: mean ADC.

CPA; cerebellopontine angle.

important to investigate the relationship between ADC value and consistency of tumors. Thus, the purpose of the present study is to evaluate the usefulness of ADC value in predicting the consistency of meningiomas.

2. Materials and methods

2.1. Patient selection

The present study protocol was approved by the institutional ethics committee, and written informed consent was waived because of the retrospective nature of the investigation. For this retrospective study, all consecutive patients with intracranial meningiomas who were referred to our institute between October 2009 and August 2010 were included. A total of 27 patients with 28 meningiomas (4 men and 23 women; mean age, 55.1 years; range, 28–74 years) were enrolled in this study. The locations of meningiomas included eight in the sphenoid ridge, six in the cerebellopontine angle (CPA), five in the convexity, four in the parasagittal region, three in the tuberculum sellae, and two in the petroclival region. Histological subtypes based on World Health Organization (WHO) classification consisted of 27 grade I tumors (meningothelial; 14, transitional; four, angiomatous; four, fibroblastic; three, psammomatous; one, and secretory; one) and one WHO grade II tumors (atypical). Calcification and intratumoral hemorrhage were not confirmed in CT and conventional MRI.

2.2. Magnetic resonance imaging examination

All patients underwent MRI with a 1.5T clinical imager (MAGNETOM Avanto; Siemens, Munich, Germany) and a quadrature head coil. All patients underwent conventional MRI including axial spine-echo T1WI sequence [repetition time (ms)/echo time (ms)=3000/90; section thickness, 5 mm; and matrix size 320×260] and an axial turbo spin-echo

T2WI sequence (repetition time (ms)/echo time (ms)=4200/108; section thickness, 5 mm; and matrix size 448×108). DWI was acquired in the axial plane, with diffusion gradients applied along the three principal orthogonal axes, in turn, by using single-shot spin-echo echo-planar (EP) sequences. The following parameters were used: matrix, 232×256; field of view, 230mm; section thickness, 5mm; intersection gap, 2.5 mm; maximum gradient strength, 33 mT/m; acquisition time, 35s; and *b* values, 0 and 1000 s/mm². ADC maps were also generated.

2.3. Image analysis

The data of DWI and ADC map were transferred to the workstation (NUMERIS/4 syngoMR B17, Siemens, Munich, Germany). Two neuroradiologists (T.K. and D.H., with ten and three years of experience of brain MRI, respectively) who were blinded to the clinical and pathological details create the regions-of-interest (ROIs) on T2WI by consensus. All ROIs were manually drawn along with the tumor contour. The position of every ROI was therefore brought back on all the other images including ADC map, T1WI, DWI with *b* values of 0 and 1000 s/mm². Cystic degeneration, flow void, bone, and susceptibility artifacts derived from air and bone were intentionally avoided. ROIs were drawn on all slices where the lesion was visualized and the minimum (ADC_{min}), maximum (ADC_{max}), and mean ADC (ADC_{mean}) values were determined.

2.4. Surgery

All patients underwent surgical resection of the meningiomas. A neurosurgeon with sixteen years of experience in brain surgery who was blinded to the analysis of ADC value evaluated the consistency of the tumors, and classified them into two groups: meningiomas with a

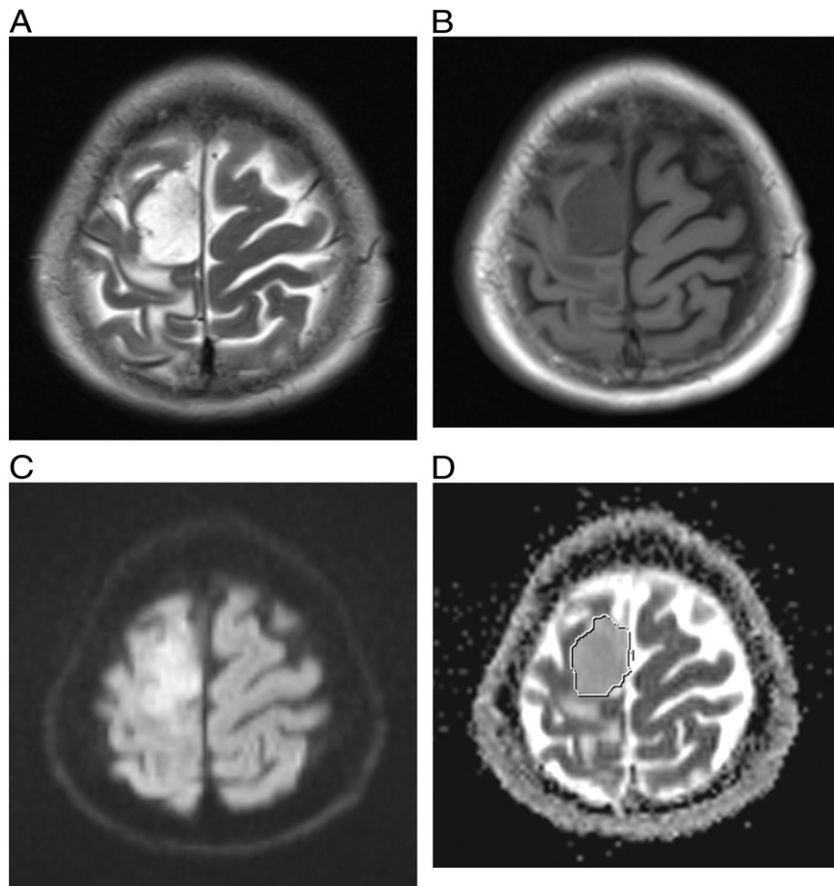


Fig. 1. A 60-year-old woman with angiomatous meningioma at right frontal parasagittal region. The tumor shows hyperintensity on T2WI (A), hypointensity on T1WI (B), and slight hyperintensity on DWI (C). The ROI was drawn around the tumor on the ADC map (D). The calculated ADC_{min} , ADC_{max} , and ADC_{mean} values were $0.66 \times 10^{-3} \text{ mm}^2/\text{s}$, $2.40 \times 10^{-3} \text{ mm}^2/\text{s}$, and $1.31 \times 10^{-3} \text{ mm}^2/\text{s}$, respectively. The ADC_{min} value was above the cut-off value ($0.64 \times 10^{-3} \text{ mm}^2/\text{s}$). Total removal was performed and the consistency was classed as soft.

“soft” consistency (removed by suction probe only) and meningiomas with a “hard” consistency (not removable through suction but excised).

2.5. Statistical analyses

Statistical analysis was achieved by statistical software (GraphPad Prism 6). Mann–Whitney U test and unpaired t test were used for analysis of ADC values between soft and hard groups. Sensitivity and specificity were calculated by receiver operating characteristics (ROC) curve analysis, and the best cut-off value was determined. The area under the curve (AUC) was elevated to assess test accuracy. In addition, all meningiomas were divided into two groups according to whether they occurred at skull base or not. All ADC values were compared between these two location groups using Mann–Whitney U test. A difference with a threshold P value of less than .05 was considered statistically significant.

3. Results

3.1. Surgical findings

At surgery, 17 meningiomas were classified as hard and 11 as soft. The hard group consisted of 10 meningothelial, two fibroblastic, two transitional, one psammomatous, one angiomatous, and one secretory meningioma. The soft group consisted of four meningothelial, three angiomatous, two transitional, one fibroblastic and one atypical. Two meningiomas demonstrated cystic components on MRI and which were confirmed at surgery.

3.2. Imaging findings and analyses

All meningiomas were clearly visualized on every MRI sequence and all ROI could be drawn accurately. Cystic degeneration and susceptibility artifacts were successfully avoided.

All ADC values of all cases are shown in Table 1. ADC_{min} , ADC_{max} , and ADC_{mean} values of all meningiomas were 0.63 ± 0.24 (range 0.11–1.49), 2.03 ± 0.65 (range 1.08–3.53), and 1.05 ± 0.27 (range 0.77–1.81) $\times 10^{-3} \text{ s}/\text{mm}^2$, respectively. For the hard group, these values were 0.52 ± 0.15 (range 0.11–0.70), 1.96 ± 0.63 (range 1.16–3.53), and 1.01 ± 0.26 (range 0.77–1.81) $\times 10^{-3} \text{ s}/\text{mm}^2$, respectively (Fig. 1) and for the soft group, these values were 0.79 ± 0.26 (range 0.54–1.49), 2.13 ± 0.71 (range 1.08–3.04), and 1.11 ± 0.29 (range 0.83–1.71) $\times 10^{-3} \text{ s}/\text{mm}^2$, respectively (Fig. 2). Statistical analysis indicated that ADC_{min} value of hard group was significantly lower than that of soft group ($P < .001$) (Fig. 3). ADC_{max} and ADC_{mean} values showed no significant difference between two groups though these values of hard group tended to be lower ($P = .52$ and $.21$, respectively). According to ADC_{min} value, the ROC curve revealed $0.64 \times 10^{-3} \text{ mm}^2/\text{s}$ as the best cut off value (Fig. 4). According to this cut-off value, sensitivity and specificity were calculated as 88% and 81%, respectively, and the AUC was 0.9.

Nineteen meningiomas were located at skull base; eight in the sphenoid ridge, six in the CPA, two in the tuberculum sellae, and two in the petroclival region (meningothelial; 10, fibroblastic; two, transitional; one, angiomatous; one, and atypical; one), and nine meningiomas were located at supratentorial region; five in the convexity and four in the parasagittal region (meningothelial; four, transitional; two, angiomatous; two, and fibroblastic; one). All ADC

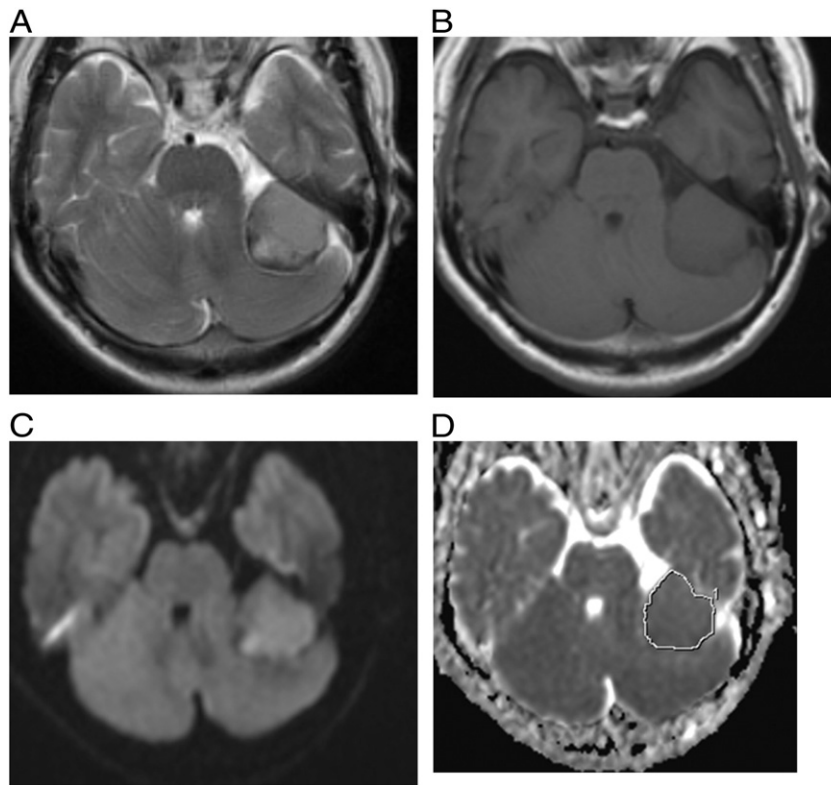


Fig. 2. A 58-year-old woman with a fibroblastic meningioma at left cerebellopontine angle. On T2WI (A), the periphery of the tumor shows hypointensity, and the inside of the tumor shows hyperintensity. The tumor shows slight hypointensity to isointensity on T1WI (B). The tumor shows hyperintensity on DWI (C). The ROI was drawn around the tumor on ADC map (D). The calculated ADC_{min} , ADC_{max} , and ADC_{mean} values were $0.45 \times 10^{-3} \text{ mm}^2/\text{s}$, $3.53 \times 10^{-3} \text{ mm}^2/\text{s}$, and $0.87 \times 10^{-3} \text{ mm}^2/\text{s}$, respectively. The ADC_{min} value was under the cut-off value ($0.64 \times 10^{-3} \text{ mm}^2/\text{s}$). Total removal was performed and the consistency was classed as hard.

values showed no significant difference between these two location groups ($P=.55, .11$, and $.75$, respectively).

4. Discussion

It has been reported that there is a significant correlation between MR signal intensity and the consistency of meningiomas. Recently, Hoover et al. and Sithinamsuwan et al. found a strong relationship between the signal intensity of T2WI and the consistency of meningiomas [24,25]. Yamaguchi et al. reported that meningiomas which showed hyperintensity on T2WI and proton density weighted images were soft, and they postulated that the water content of meningiomas is an important factor related to consistency [21]. Maiuri et al. reported that meningiomas with more hyperintensity than the cortex on T2WI were usually soft, more vascular, and more frequently were of the syncytial or angioblastic subtype, whereas meningiomas with more hypointensity than the cortex on T2WI tended to be hard and more frequently of the fibroblastic subtype [8]. These reports concluded that the amount of water or fibrous tissue resulted in a soft or hard consistency, and hyperintensity or hypointensity on T2WI, respectively [8,21,24,25].

However, this correlation has not been consistently demonstrated. Carpeggiani et al. did not find any statistically significant correlation between signal intensity and the consistency of meningioma, although they agreed that hyperintense meningioma on T2WI was unlikely to be fibroblastic or hard [12]. Besides, Kasoff et al. didn't find any relationship between MRI findings with the consistency and water content of meningiomas [11].

Tumor cellularity and the amount of fibrous tissue are important factors of tumor consistency. Meningioma cells are characterized by interdigitations connected with junctional complexes and extracellular cisterns, and it is supposed that meningiomas with higher

cellularity have stronger cell adhesion [21]. Fibrous tissue and high cellularity with a low nucleus-to-cytoplasm ratio reduce the signal intensity on T2WI, whereas extracellular space with interstitial fluid may increase the signal intensity on T2WI. Each of these mechanisms can have a different contribution to signal intensity on T2WI and may therefore limit the diagnostic utility in predicting the consistency. It has been suggested that the ADC value inversely correlates with tumor cellularity and the amount of fibrous tissue within heterogeneous tumors [9,14,15,26]. Thus, it is supposed that tumors, including meningiomas, with low ADC value have a hard consistency. In this

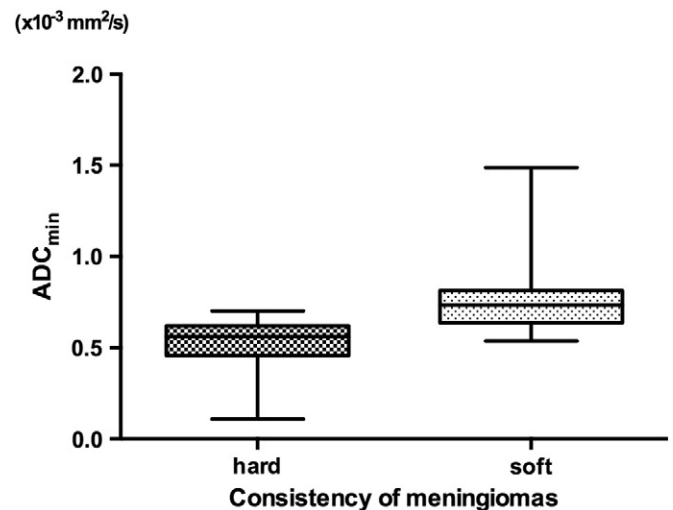


Fig. 3. Box plots showing the consistency of the meningioma and the ADC_{min} value. ADC_{min} value in the hard group was significantly lower ($P<.001$).

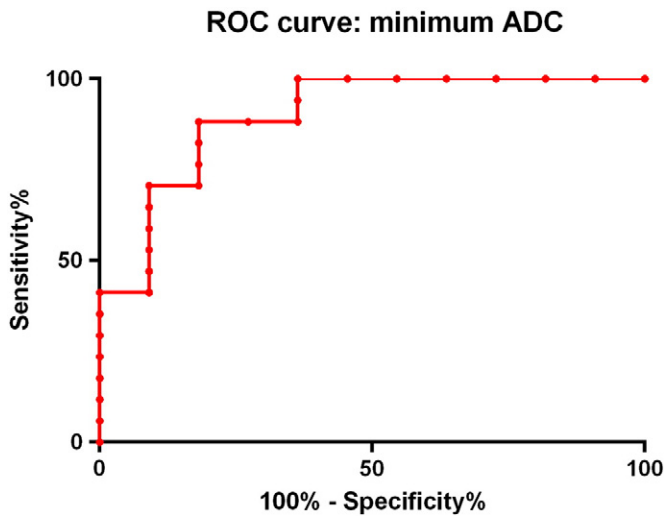


Fig. 4. Graph shows the ROC curves of ADC_{min} . The ROC curve calculated the best cut off value as $0.64 \times 10^{-3} \text{ mm}^2/\text{s}$. For this cut-off value, sensitivity and specificity were calculated 88% and 81%, respectively. The AUC was 0.9.

study, the minimum ADC values of hard group showed significantly lower ADC values than those of soft group, which consistent with this theory. Maximum ADC values and mean ADC values, on the other hand, showed no significant difference between hard and soft groups though mean ADC were reported to be related to some histologic subtypes [27]. It is because we divided meningiomas into soft or hard group according to if they were completely resected by suction probe only. In this classification, if a small component of meningioma could not be removed by suction probe only, the meningioma was classified as “hard” group even though most parts were easily removed. Though this division is not directly associated with whole histologic feature, it is useful to determine which surgical devices will be needed for complete resection.

Recently, Hoover et al. reported that T1WI and T2WI predicted the consistency of meningiomas, but DWI and ADC maps were not correlated with tumor consistency [24]. They, however, performed only qualitative analysis and did not measure ADC values of the meningioma. In contrast, we performed a quantitative analysis using ROIs. These ROIs were constructed by contouring the tumor with all slices and avoiding cystic degeneration, flow void, bone, and susceptibility artifacts. Thus, this method can better reflect the entire tumor tissue.

As hemosiderin deposition was not confirmed in present study, it is not common in meningioma unlike pituitary macroadenomas, in which intratumoral hemorrhage often occurs and results in preventing calculating ADC values accurately [17]. Thus, intrinsic susceptibility artifacts were less common in meningiomas, excepting the cases with calcification.

On DWI, abnormal signal change and spatial distortion often occurs by the susceptibility artifacts derived by air, bone, and hemorrhage, which could result in showing inadequate ADC values. Though meningiomas occur in supratentorial region more commonly than in skull base [4] where susceptibility artifacts often exist [28], about two thirds of cases were located at skull base in the present study. Because there was no significant difference in ADC values between these two location groups, it is supposed that potential susceptibility artifacts did not significantly affect the ADC values.

Present study has several limitations. The principle limitation of our study is its relatively small number of patients. Second, because there was a lack of direct histopathological correlation with ADC values, we could not clarify which was the main factor accounting for decreasing ADC values, high cellularity or rich fibrous tissue. Third, all ROIs were drawn manually and were susceptible to bias. Two blinded

observers, however, drew ROIs by consensus, which should have minimized it. Fourth, all DWI were performed by using EP sequences, which often suffered by susceptibility artifacts at skull base. As mentioned above, we drew ROIs avoiding artifacts, and ADC values showed no significant difference between skull base lesion and supratentorial lesion. Thus, it is supposed that there was little influence that intrinsic susceptibility artifact affected ADC values in this study. Further study using advanced DWI technique including readout-segmented EP imaging [29], periodically rotated overlapping parallel lines with enhanced reconstruction (PROPELLER) DWI [17], and 3D turbo field echo with diffusion-sensitized driven-equilibrium preparation [30], which has higher spatial resolution and fewer susceptibility artifacts, might elucidate the relationship between ADC values and meningioma consistency. Finally, we didn't confirm prospectively if minimum ADC value would really give surgeon useful information in making decision of management. There is still an overlap of the ADC values between two groups, and it could be misleading in determining consistency. It might be more useful to combine the results of signal intensity of other sequences including T2WI, T1WI, and so on, and further studies are needed.

5. Conclusions

The present study suggests that the minimum ADC value can be a promising tool to predict the consistency of intracranial meningiomas. Meningiomas with low minimum ADC are considered to have a hard consistency. It is very important and beneficial to predict the meningioma consistency for surgical planning and selection of the surgical devices, especially if the tumors are located in complex regions. Because DWI is available in many institutes, the minimum ADC may be a tool for predicting the consistency of meningiomas. Furthermore, with inclusion of more study cases and analysis across modalities, ADC values may help select cases for preoperative embolization in future.

Conflicts of interest

None.

Acknowledgments

We received no acknowledgement of grants, disclosures, or other assistance.

References

- [1] Dobes M, Khurana VG, Shadbolt B, Jain S, Smith SF, Smee R, Dexter M, Cook R. Increasing incidence of glioblastoma multiforme and meningioma, and decreasing incidence of Schwannoma (2000–2008): findings of a multicenter Australian study. *Surg Neurol Int* 2011;2:176. <http://dx.doi.org/10.4103/2152-7806.90696>.
- [2] Hoffman SPJ, McCarthy BJ. Temporal trends in incidence of primary brain tumors in the United States, 1985–1999. *Neuro Oncol* 2009;8:27–37.
- [3] Klæboe L, Lonn S, Scheie D, Auvinen A, Christensen HC, Feychting M, Johansen C, Salminen T, Tynes T. Incidence of intracranial meningiomas in Denmark, Finland, Norway and Sweden, 1968–1997. *Int J Cancer* 2005;20:996–1001.
- [4] Belinda A, Campbell MBBS, Jhamb A, Manguir JA, Toyota B, Roy M. Meningiomas in 2009: controversies and future challenges. *Am J Clin Oncol* 2009;32:73–85.
- [5] Majda M, Thurnher MD, editors. *Diagnostic imaging: brain*. 2nd ed. Salt Lake City: Amirsy; 2010.
- [6] Eis M, Els T, Hoehn-Berlage M, Hossmann KA. Quantitative diffusion MR imaging of cerebral tumor and edema. *Acta Neurochir Suppl (Wien)* 1994;60:344–6.
- [7] Chen TC, Zee CS, Miller CA, Weiss MH, Tang G, Chin L, Levy ML, Apuzzo ML. Magnetic resonance imaging and pathological correlates of meningiomas. *Neurosurgery* 1992;31:1015–22.
- [8] Maiuri F, Iaconetta G, de Divitiis O, Cirillo S, Di Salle F, De Caro ML. Intracranial meningiomas: correlations between MR imaging and histology. *Eur J Radiol* 1997;31:69–75.
- [9] Guo AC, Cummings TJ, Dash RC, Provenzale JM. Lymphomas and high-grade astrocytomas: comparison of water diffusibility and histologic characteristics. *Radiology* 2002;224:177–83.
- [10] Castillo M, Smith JK, Kwock L, Wilber K. Apparent diffusion coefficients in the evaluation of high-grade cerebral gliomas. *AJNR Am J Neuroradiol* 2001;22:60–4.

- [11] Eis M, Els T, Hoehn-Berlage M. High resolution quantitative relaxation and diffusion MRI on three different experimental brain tumors in rat. *Magn Reson Med* 1995;34:835–44.
- [12] Eis M, Els T, Hoehn-Berlage M, Hossmann KA. Quantitative diffusion MR imaging of cerebral tumor and oedema. *Acta Neurochir Suppl (Wien)* 1994;60:344–6.
- [13] Gauvain KM, McKinstry RC, Mukherjee P, Perry A, Neil JJ, Kaufman BA, Hayashi RJ. Evaluating pediatric brain tumor cellularity with diffusion-tensor imaging. *AJR Am J Roentgenol* 2001;177:449–54.
- [14] Kono K, Inoue Y, Nakayama K, Shakudo M, Morino M, Ohata K, Wakasa K, Yamada R. The role of diffusion-weighted imaging in patients with brain tumors. *AJNR Am J Neuroradiol* 2001;22:1081–8.
- [15] Sugahara T, Korogi Y, Kochi M, Ikushima I, Shigematu Y, Hirai T, Okuda T, Liang L, Ge Y, Komohara Y, Ushio Y, Takahashi M. Usefulness of diffusion-weighted MRI with echo-planar technique in the evaluation of cellularity in gliomas. *J Magn Reson Imaging* 1999;9:53–60.
- [16] Fujimoto K, Tonan T, Azuma S, Kage M, Nakashima O, Johkoh T, Hayabuchi N, Okuda K, Kawaguchi T, Sata M, Qayyum A. Evaluation of the mean and entropy of apparent diffusion coefficient values in chronic hepatitis C: correlation with pathologic fibrosis stage and inflammatory activity grade. *Radiology* 2011;258(3):739–48.
- [17] Mahmoud OM, Tominaga A, Amatya VJ, Ohtaki M, Sugiyama K, Sakoguchi T, Kinoshita Y, Takeshima Y, Abe N, Akiyama Y, El-Ghoriyan AI, Abd Alla AK, El-Sharkawy MA, Arita K, Kurisu K, Yamasaki F. Role of PROPELLER diffusion-weighted imaging and apparent diffusion coefficient in the evaluation of pituitary adenomas. *Eur J Radiol* 2011;80(2):412–7.
- [18] Kashimura H, Inoue T, Ogasawara K, Arai H, Otawara Y, Kanbara Y, Ogawa A. Prediction of meningioma consistency using fractional anisotropy value measured by magnetic resonance imaging. *J Neurosurg* 2007;107(4):784–7.
- [19] Le Bihan D, Mangin JF, Poupon C, Clark CA, Pappata S, Molko N, Chabriat H. Diffusion tensor imaging: concepts and applications. *J Magn Reson Imaging* 2001;13(4):534–46.
- [20] Muthupillai R, Lomas DJ, Rossman PJ, Greenleaf JF, Manduca A, Ehman RL. Magnetic resonance elastography by direct visualization of propagating acoustic strain waves. *Science* 1995;269:1854–7.
- [21] Muthupillai R, Rossman PJ, Lomas DJ, Greenleaf JF, Riederer SJ, Ehman RL. Magnetic resonance imaging of transverse acoustic strain waves. *Magn Reson Med* 1996;36:266–74.
- [22] Pierpaoli C, Basser PJ. Toward a quantitative assessment of diffusion anisotropy. *Magn Reson Med* 1996;36(6):893–906.
- [23] Tropine A, Dellani PD, Glaser M, Bohl J, Plöner T, Vucurevic G, Perneczky A, Stoeter P. Differentiation of fibroblastic meningiomas from other benign subtypes using diffusion tensor imaging. *J Magn Reson Imaging* 2007;25(4):703–8.
- [24] Hoover JM, Morris JM, Meyer FB. Use of preoperative magnetic resonance imaging T1 and T2 sequences to determine intraoperative meningioma consistency. *Surg Neurol Int* 2011;2:142. <http://dx.doi.org/10.4103/2152-7806.85983>.
- [25] Sitthinamsuwan B, Khampalikit I, Nunta-aree S, Srirabheebhat P, Witthiwej T, Nitising A. Predictors of meningioma consistency: A study in 243 consecutive cases. *Acta Neurochir (Wien)* 2012;154(8):1383–9.
- [26] Higano S, Yun X, Kumabe T, Watanabe M, Mugikura S, Umetsu A, Sato A, Yamada T, Takahashi S. Malignant astrocytic tumors: clinical importance of apparent diffusion coefficient in prediction of grade and prognosis. *Radiology* 2006;241:839–46.
- [27] Yin B, Liu L, Ahang BY, Li YX, Geng DY. Correlating apparent diffusion coefficients with histopathologic findings on meningiomas. *Eur J Radiol* 2012;81(12):4050–6.
- [28] Le Bihan D, Poupon C, Amadon A, Lethimonnier F. Artifacts and pitfalls in diffusion MRI. *J Magn Reson Imaging* 2006;24(3):478–88 [Review].
- [29] Holdsworth SJ, Yeom K, Skare S, Gentles AJ, Barnes PD, Bammer R. Clinical application of readout-segmented-echo-planar imaging for diffusion-weighted imaging in pediatric brain. *AJNR Am J Neuroradiol* 2011;32(7):1274–9.
- [30] Hiwatashi A, Yoshiura T, Togao K, Yamashita K, Kikuchi K, Kobayashi M, Ohga S, Sonoda S, Honda H, Obara M. Evaluation of diffusivity in the anterior lobe of the pituitary gland: 3D turbo field echo with diffusion-sensitized driven-equilibrium preparation. *AJNR Am J Neuroradiol* 2014;35:95–8.

Enhanced expression of proapoptotic and autophagic proteins involved in the cell death of glioblastoma induced by synthetic glycans

Laboratory investigation

AHMAD FARIED, M.D., PH.D.,¹ MUHAMMAD ZAFRULLAH ARIFIN, M.D., PH.D.,¹
SHOGO ISHIUCHI, M.D., PH.D.,² HIROYUKI KUWANO, M.D., PH.D.,³ AND SHIN YAZAWA, PH.D.^{3,4}

¹Department of Neurosurgery, Faculty of Medicine, Universitas Padjadjaran–Dr. Hasan Sadikin Hospital, Bandung, Indonesia; ²Department of Neurosurgery, Faculty of Clinical Medicine, the University of Ryukyus, Nakagami-gun, Okinawa; ³Department of General Surgical Science, Faculty of Medicine, Gunma University, Maebashi; and ⁴Tokushima Research Institute, Otsuka Pharmaceutical Co. Ltd., Tokushima, Japan

Object. Glioblastoma is the most aggressive malignant brain tumor, and overall patient survival has not been prolonged even by conventional therapies. Previously, the authors found that chemically synthesized glycans could be anticancer agents against growth of a series of cancer cells. In this study, the authors examined the effects of glycans on the growth of glioblastoma cells both in vitro and in vivo.

Methods. The authors investigated not only the occurrence of changes in the cell signaling molecules and expression levels of various proteins related to cell death, but also a mouse model involving the injection of glioblastoma cells following the administration of synthetic glycans.

Results. Synthetic glycans inhibited the growth of glioblastoma cells, induced the apoptosis of the cells with cleaved poly (adenosine diphosphate-ribose) polymerase (PARP) expression and DNA fragmentation, and also caused autophagy, as shown by the detection of autophagosome proteins and monodansylcadaverine staining. Furthermore, tumor growth in the in vivo mouse model was significantly inhibited. A dramatic induction of programmed cell death was found in glioblastoma cells after treatment with synthetic glycans.

Conclusions. These results suggest that synthetic glycans could be a promising novel anticancer agent for performing chemotherapy against glioblastoma.

(<http://thejns.org/doi/abs/10.3171/2014.1.JNS131534>)

KEY WORDS • synthetic glycan • glioblastoma • apoptosis • autophagy • oncology

GLIOLASTOMA is the most aggressive and lethal malignancy of the CNS, and patients with glioblastoma have an average life expectancy of 1 year after the standard treatment of surgery followed by radiation therapy.^{26,45} Recently, clinical studies have shown

Abbreviations used in this paper: Akt = protein kinase B; AMPA = α -amino-3-hydroxy-5-methyl-4-isoxazolepropionic acid; CPI = cell proliferation inhibition; HP- β -CD = hydroxypropyl- β -cyclodextrin; Gal β Chol = D-galactose β cholestanol; GChol = GlcNAc β Chol; GGChol = GlcNAc β 1,3 Gal β Chol; GlcNAc β 1,3 = N-acetyl-D-glucosamine β 1,3; GluR1 = glutamate receptor 1; GluR4 = glutamate receptor 4; HO342 = Hoechst 33342; MDC = monodansylcadaverine; mTOR = mammalian target of rapamycin; PARP = poly (adenosine diphosphate-ribose) polymerase; PI3K = phosphatidylinositol 3-kinase; Z-VAD-FMK = benzyloxycarbonyl-Val-Ala-Asp(OMe)-fluoromethylketone.

that chemotherapy in addition to radiation therapy could increase patient survival up to 2 years.⁴⁵ The continuing problems caused by glioblastoma and the failure of conventional therapy for this advanced invasive brain tumor indicate that novel strategies and anticancer drugs are critically needed to improve the prognosis.

Glioblastoma cells are naturally resistant to cell death,^{16,26} which has been considered to be attributable to the activation of phosphatidylinositol 3-kinase (PI3K) by growth factors and the subsequent hyperactivation of its downstream targets, the serine/threonine kinases protein kinase B (Akt) and mammalian target of rapamycin (mTOR). These targets are known to release a variety of

This article contains some figures that are displayed in color online but in black-and-white in the print edition.

antiapoptotic signals, thereby promoting the proliferation of the tumor cells.^{26,34,39} Growing evidence is accumulating that glioblastoma cells exploit glutamate for their proliferation and migration ability. The released glutamate may stimulate glioblastoma cell growth and migration through the autocrine and/or paracrine activation of glutamate receptors.^{20,21} In addition, the expression of Rho GTPase family members has been demonstrated in a wide variety of malignancies^{9,12,18,23} and in high-grade glioma as a hallmark of cell migration and as a predictor of the clinical prognosis.⁴⁷

Programmed cell death plays an important role during tissue development and homeostasis. Aberrations in this process result in the pathology of numerous disorders, such as malignancy. Apoptosis is the most common form of programmed cell death, but recently, alternative cell death programs have received increased attention, with autophagy proposed as an important nonapoptotic cell death mechanism.^{6,33}

In our previous studies, using chemically synthesized glycans consisting of sugar cholestanols with mono-, di-, and trisaccharides attached to cholestanols, we showed both strong inhibitory activity against the proliferation of a series of mouse and human cancer cells from the digestive system and antitumor effects in a mouse model of peritoneal dissemination.^{8,14,15} The sugar cholestanols added to the cell culture were rapidly taken up via the lipid rafts/microdomains on the cell surface.¹⁵ The uptake of sugar cholestanols in mitochondria increased gradually and was followed by the activation of apoptotic signals via the caspase cascade, leading to apoptotic cell death.^{8,14,15} Furthermore, the examination of sugar cholestanols in a mouse model of peritoneal dissemination showed a dramatic reduction of tumor growth and a prolonged survival time of the mice.¹⁵ The sugar cholestanols described in our previous studies, therefore, appeared to have clinical potential as novel anticancer agents. However, the cell death pathways in malignant glioma cells induced by the same compounds remain an open question. In this study, we investigated the programmed cell death induced by the sugar cholestanols in glioblastoma cells and its anticancer effect on growth in nude mice.

Methods

Cell Lines and Culture Condition

Human glioblastoma cell lines, CGNH-89 and CGNH-NM, were established as described previously.^{19,20} The morphology of CGNH cells is epithelial and adherent type, and their doubling time is 24 hours. CGNH cells were established through resection from the tumor at the right frontal lobe of female patients according to the explant method by Nichols et al.³⁶ It has been demonstrated that the CGNH cells have glioblastoma morphological characteristics, and they grow very fast (highly cellular) and are relatively monotonous, while some are multinucleated giant cells with slight nuclear pleomorphism, marked atypical nucleus, and brisk mitotic activity.^{19,20} The cells were maintained at 37°C in DMEM (Nissui) supplemented with 10% fetal bovine serum (Invitrogen) and 3% L-glutamine in a humidified atmosphere of 5% CO₂ in air. When they

were confluent, the cells were exposed in 0.05% trypsin and subcultured in the same growth medium.

Compounds

N-acetyl-D-glucosamine (GlcNAc) β1,3 D-galactose (Gal) β cholestanol, or GGChol, and GlcNAc β cholestanol, or GChol, were synthesized and prepared^{13,15} as an inclusion complexation with 20% of hydroxypropyl-β-cyclodextrin (HP-β-CD; BICO) and used for the experiment as previously described.^{8,15}

Antibodies and Chemical Reagents

Anti-GluR1 (glutamate receptor 1) and GluR4 (glutamate receptor 4) were obtained from Chemicon. Anti-RhoA, RhoC, Beclin-1, and LC3 were obtained from Santa Cruz Biotech, Inc. Anti-pAkt at ser473, pmTOR at ser2448, p53 at ser46, Bcl-2 family, caspase family, and poly (adenosine diphosphate-ribose) polymerase (PARP) were obtained from Cell Signaling. 3-Methyladenine (3-MA; Sigma), was used as an inhibitor of autophagy. 3-MA (30 mg) was dissolved with 1 ml dH₂O to make a 200 mM stock solution and kept at room temperature. Benzoyloxycarbonyl-Val-Ala-Asp(OMe)-fluoromethylketone (Z-VAD-FMK, or just Z-VAD; BD Biosciences), a general caspase inhibitor, was used to inhibit apoptosis. Z-VAD was dissolved in dimethylsulfoxide for a stock solution. And 1 mM of 3-MA and 10 μM of Z-VAD were diluted separately in DMEM to obtain the desired concentration. The autofluorescent agent monodansylcadaverine (MDC; Sigma) was introduced as a specific autophagolysosome marker to analyze the autophagic process.³² The fluorescence of MDC has been reported to be a specific marker for autophagic vacuoles.¹ Monodansylcadaverine was dissolved in methanol (10 mg/ml) and used to observe autophagy.

Cell Proliferation Inhibition and Nuclear Fragmentation Assays

Cell proliferation inhibition with each compound was conducted in the presence of serially diluted compounds as described previously.^{8,15} DNA binding dyes, Hoechst 33342 (HO342), in addition to propidium iodide fluorescence, were used for determination of apoptosis.¹⁷ Cells were exposed to HO342 (10 μM) and propidium iodide (10 μM), and each fluorescence intensity was examined using a fluorescence microscope with ultraviolet excitation at 340–380 nm. The apoptotic index (AI) was calculated as follows:

$$\text{AI} = \frac{\text{apoptotic cell number}}{\text{apoptotic cell number} + \text{necrotic cell number} + \text{viable cell number}} \times 100\%$$

Protein Extraction and Western Blot Analysis

All cells were harvested at approximately 80% confluent growth. Protein concentrations of the cell lysate were determined with a bicinchoninic acid protein assay kit (Pierce) using bovine serum albumin as a standard. Each sample (50 μg protein/line) was run on a 5%–20% ReadyGel (Bio-Rad) and the gel was then electrotransferred to a hybrid-enhanced chemiluminescence nitrocellulose

Cell death of glioblastoma induced by glycans

membrane (Amersham Pharmacia Biotech). Changes in expression levels of corresponding (apoptosis and autophagy) proteins after treatment with sugar cholestanol were analyzed by Western blotting; β -actin was used as a loading control. Bands on the membrane were detected using an enhanced chemiluminescence detection system, and horizontal scanning densitometry was performed using Photoshop software (version 3.0, Adobe), and analyzed by Quantity One software (BioRad).

Analysis of Autophagy

The analysis of autophagy was performed with the aid of MDC and counted as previously described.³² Autophagic vacuoles were labeled with MDC, and the fluorescent images were obtained with an epifluorescence microscope (BX-50, Olympus). The quantification of intracellular MDC accumulation was measured by fluorometry. Cells (2×10^4) were incubated with 0.05 mM MDC in phosphate-buffered saline at 37°C for 10 minutes and collected in 10 mM Tris-HCl, pH 8.0, containing 0.1% Triton X-100. Fluorescence was measured at a 380-nm excitation wavelength with a 530-nm emission filter, using an MTP-600 microplate reader (Corona Electric). Monodansylcadaverine expression was measured using a relative unit to show the ratio of the amount on intensity from fluorescence imaging.

Antitumor Effect of Sugar Cholestanols on Nude Mice Injected With CGNH-89 Cells

The effect of sugar cholestanols on CGNH-89 cell growth was evaluated quantitatively in a subcutaneous tumor. Cell suspensions (2×10^7 cells/200 μ l) were injected subcutaneously in the flanks of 5- to 6-week-old nude mice (Clea Laboratories). One hundred microliters of 2 μ mol of GChol dissolved in HP- β -CD was administered intratumorally 3 times (at 14, 15, and 16 days) after tumor inoculation with a 27-gauge needle. The same treatment of HP- β -CD without GChol was conducted as control. Tumor volume was calculated as follows: (length \times width²)/2.

At the end of each experiment, tumor tissues were subjected to histological analysis. Five mice were used for each group, and the experiment was approved by the Animal Care and Experimentation Committee of Gunma University. Experiments using patient tissues from glioblastoma cells were approved by the Ethical Committee of Gunma University.

Statistical Analysis

Statistical analysis was performed using StatView software (version 5.0, SAS Institute). Differences were considered significant when p was < 0.05 .

Results

Cell Proliferation Inhibition of Glioblastoma Cells by Sugar Cholestanols

The effects of sugar cholestanols on the viability of glioblastoma cells were evaluated at various concentrations. Sugar cholestanols such as GGChol and GChol showed considerable inhibiting activities against the pro-

liferation of glioblastoma cells in a dose-dependent manner (Fig. 1). However, β Chol itself, without the sugar moiety, showed very low activity only at a high concentration in CGNH cells (data not shown). The minimum concentrations of sugar cholestanols producing 50% cell proliferation inhibition (CPI₅₀) were determined in the glioblastoma cells, and no clear differences were observed (Table 1). The sugar cholestanols clearly induced cell death in glioblastoma cells.

Nuclear Fragmentation

Nuclear fragmentation was clearly observed in CGNH cells treated with GGChol but not in the control cells (Fig. 2 left). Staining of the glioblastoma cells (CGNH-89 and CGNH-NM) with HO342 and propidium iodide indicated that GGChol induced nuclear fragmentation (a hallmark of apoptosis) in approximately 17% and 23% of the total cells, respectively, and were counted as apoptotic (Fig. 2 right).

Western Blot Analysis of Caspase Cascade and PARP Activation

Caspase signaling pathways consisting of a death receptor-dependent extrinsic pathway and death receptor-independent intrinsic pathway were examined in the glioblastoma cells treated with GGChol. The expression levels of active caspase-8 for the extrinsic pathway, caspase-9 for the intrinsic pathway, and caspase-3 were found to increase in the CGNH-89 and CGNH-NM cells in a time-dependent manner (Fig. 3). The expression levels of PARP, one of the best biomarkers of apoptosis, were analyzed in CGNH cells during the 24 hours after the treatment with GGChol. The N-terminal fragment of PARP, possessing an 89-kDa peptide cleaved from the full-sized PARP (116 kDa), was detected as early as 2 hours in the CGNH cells after the treatment with sugar cholestanols (Fig. 3). These results suggested that GGChol induced apoptotic cell death through both extrinsic and intrinsic pathways.

Analysis of Autophagy, Apoptosis, and the Inhibition of Both

We examined the changes in autophagy activity in both CGNH-89 and CGNH-NM cells treated with GGChol. The treatment of both cell types with GGChol induced not only apoptosis but also an autophagic response (Fig. 4). In both cell types, the number of distinct dot-like structures distributed within the cytoplasm or localized in the perinuclear regions was higher than in the control (Fig. 4A and B, left). The level of MDC incorporated into the CGNH-89 and CGNH-NM cells was increased 1.4- and 1.5-fold, respectively, after being treated with GGChol compared with that in the untreated cells (Fig. 4A and B, right). The cell viability of glioblastoma cells was reduced in the presence of GGChol up to 60% but was restored after the addition of 3-MA and Z-VAD to the culture medium (Fig. 4C). Our results showed that 3-MA and Z-VAD can block autophagy and apoptosis from 17%–20% and 38%–41%, respectively. The combination of inhibitors against both autophagy and apoptosis can fully block the cell death induced by GGChol (45%–

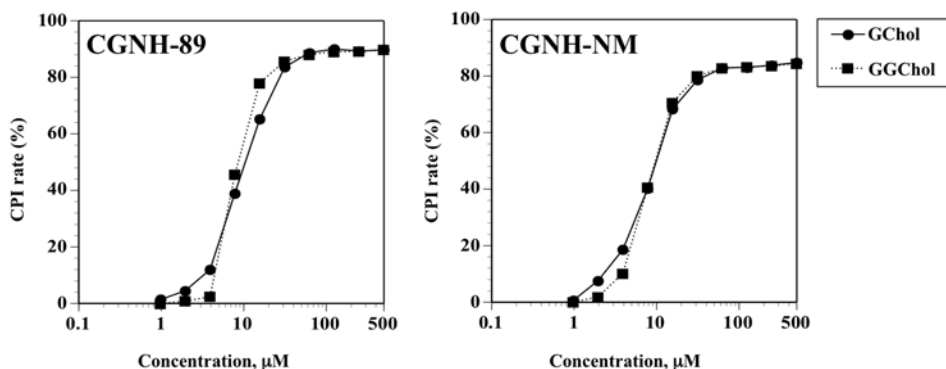


Fig. 1. Line graphs showing the effect of sugar cholestanols on the viability of glioblastoma cells. The CGNH-89 and CGNH-NM cells were treated with various concentrations of sugar cholestanols for 24 hours.

48% increase). When 3-MA and Z-VAD were added at the same time to the cell culture, the cell viability in the GGChol-treated cells was as high as that of the untreated control cells. However, no effect was observed when either agent was added individually to the cell culture (Fig. 4C).

Western Blot Analysis of the Bcl-2 Family

The expression levels of Bcl-2 family members, consisting of both proapoptosis and antiapoptosis factors, were then analyzed in the CGNH cells treated with GGChols. A slightly increased expression of Bax (proapoptosis) was detected in the CGNH-89 and CGNH-NM cells in a time-dependent manner, and a slightly decreased expression of Bcl-xL (antiapoptosis) was detected in the same cells (Fig. 5). We also evaluated the expression level of p53 (ser46), one of the initiators that activates Bax and/or downregulates Bcl-xL. Our results showed that glioblastoma cells treated with GGChol increased the expression of p53 (ser46) in a time-dependent manner (Fig. 5).

Western Blot Analysis of Autophagy

Using Western blot analysis and MDC staining, we found that GGChol increased the expression of apoptosis-related proteins and slightly increased the expression of LC3-II and Beclin-1 (Fig. 5). All these results suggest that sugar cholestanols induced both apoptosis and autophagic cell death in glioblastoma cells.

Western Blot Analysis of Survival Pathways

The expression of survival signaling proteins was

TABLE 1: Minimum amounts of each compound producing 50% cell proliferation inhibition of various cells*

Compounds	CPI ₅₀ (µM)	
	CGNH-89	CGNH-NM
GGChol	14.8	15.6
GChol	15.6	17.2
cholestanol	>1000	>1000

* The 3(4,5-dimethylthiazol-2-yl)2,5-diphenyltetrazolium bromide (MTT) assay was conducted after 24 hours of incubation under the presence of each compound diluted from 500 µM to 0.98 µM (in a gradual manner).

evaluated in glioblastoma cells in response to sugar cholestanols. The treatment of both CGNH cell types with GGChol indicated inhibition of Akt activation and expression of both phosphorylated Akt (ser473) and phosphorylated mTOR (ser2448), the downstream targets of Akt in glioblastoma cells (Fig. 6A). The expression levels of the upstream molecules related to Akt/mTOR were also analyzed in CGNH cells treated with GGChol, and the decreased expression of both GluR1 and GluR4 was detected in CGNH cells treated with GGChol in a time-dependent manner (Fig. 6A). However, the expression levels of RhoA and RhoC in CGNH cells treated with GGChol were revealed to be suppressed in a time-dependent manner (Fig. 6B).

Antitumor Effect of Sugar Cholestanols in a Mouse Model

Nude mice were subcutaneously inoculated with CGNH-89 cells and tumors formed within 2 weeks in all

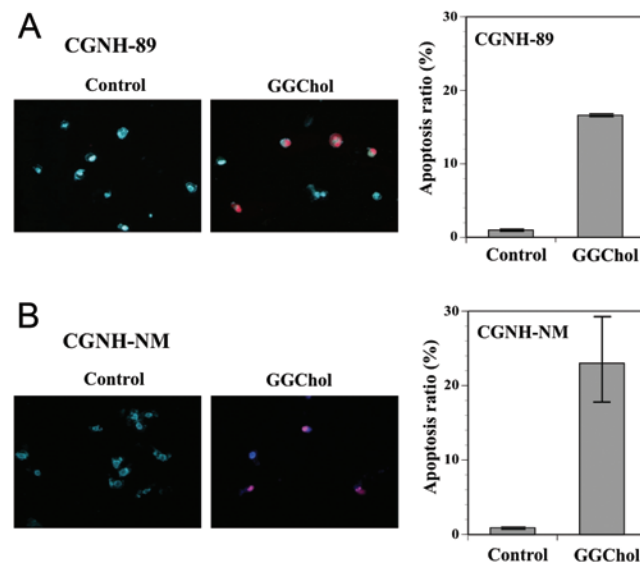


Fig. 2. Left: Induction of apoptotic cell death in CGNH-89 (A) and CGNH-NM (B) cells after treatment with GGChol. The cells were analyzed by the HO342 combined with propidium iodide assay. Original magnification ×200. Right: The apoptosis index (mean ± SEM) was calculated in each cell line. All results were from 3 independent experiments.

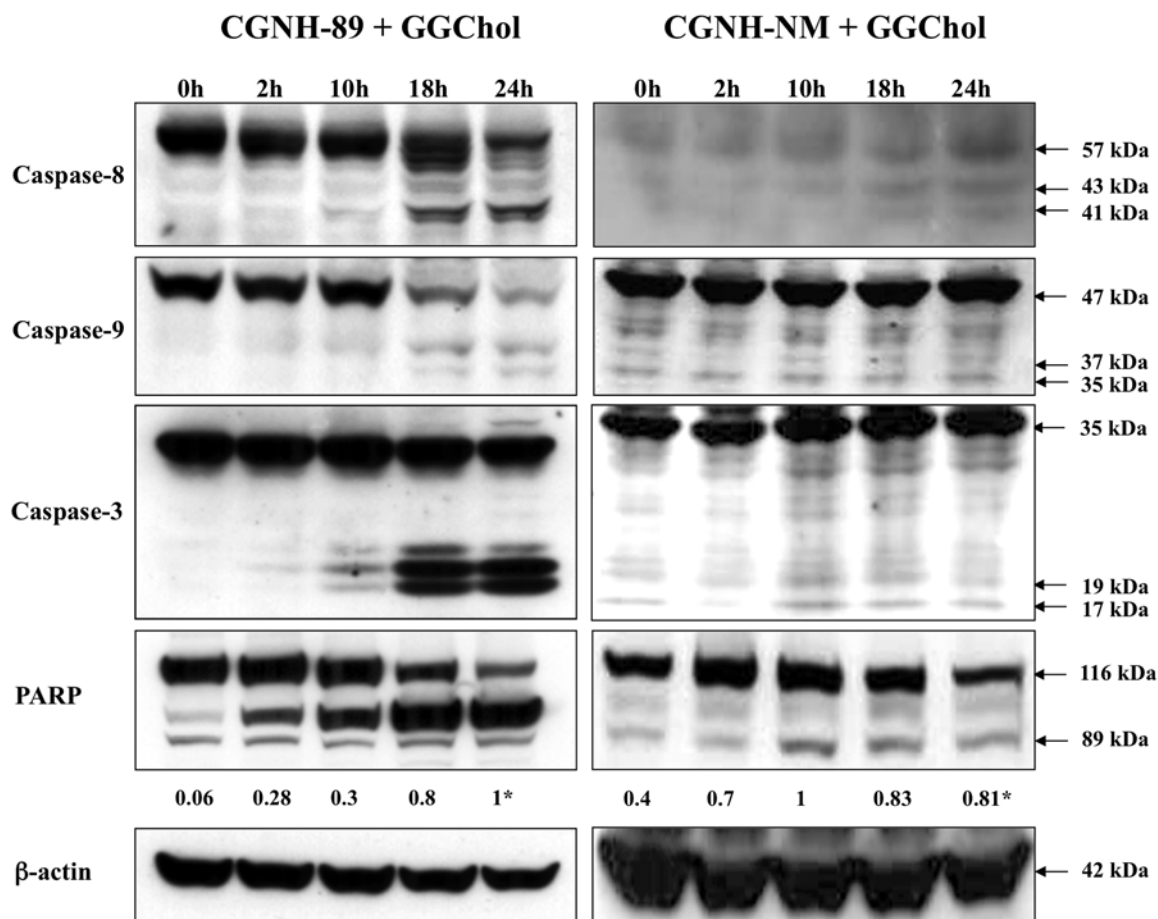


Fig. 3. Western blot analysis of glioblastoma cells treated with GGChol. The cells were treated with 30 μ M of GGChol for 24 hours, and the values given below the caspase-8, -9, -3, and PARP figures indicate the calculation of the active form band (41–43 kDa, 35–37 kDa, 17–19 kDa, and 89 kDa, respectively) after normalization of its expression to that of β -actin, shown as a percentage compared with the control. Asterisk = significant increase for the active form of cleaved PARP (89 kDa) measured using densitometric analysis.

mice. Tumor formation was significantly suppressed ($p < 0.05$) in the mice treated with GChol in HP- β -CD intratumorally 3 times at 14, 15, and 16 days after inoculation of tumor cells. However, no significant suppression was observed in the mice treated only with HP- β -CD (Fig. 7). The histological analysis of GChol-treated mice revealed the presence of high degrees of tumor anaplasia including nuclear and cytoplasmic pleomorphism, tumor necrosis, and vascular proliferation. However, in the control mice, large numbers of mitotic cells were observed (data not shown), as hallmarks of the glioblastoma cells.

Discussion

Temozolomide is commonly used in the treatment of primary or recurrent high-grade gliomas, including anaplastic astrocytoma and glioblastoma.^{2,48} To date, the prognosis of patients with malignant gliomas has been poor.⁴ It is clear that tumor cells with drug-resistant ability will not respond to chemotherapy treatment. The mechanism by which temozolomide mediates cell death in malignant tumor cells has been characterized, and it was shown to induce autophagy, not apoptosis, in glioblastoma.²⁴ In the

cancer field, autophagy is a new concept for the defense mechanisms of malignant cells,^{38,40} and they are eliminated, in some cases, due to the induction of a nonapoptotic mechanism, also known as autophagic cell death.³ However, the triggers for the induction of autophagy and apoptosis and their roles remain unclear.

In our previous studies, novel glycans consisting of a series of sugar cholestanols were chemically synthesized and evaluated as anticancer drugs in both in vitro and in vivo experiments.^{8,14,15} In this study, the expression levels of a series of molecules related to programmed cell death (apoptosis and autophagy) were investigated in glioblastoma cells treated with the same sugar cholestanols. We used CGNH-type glioblastoma cells, cell lines showing epithelial morphology and adhesive capacity. These cell lines possess glial fibrillary acidic protein, vimentin, A2B5, O4, and myelin basic protein.⁴² The mRNAs for the glutamate-AMPA receptors (GluR1 and GluR4) were analyzed in CGNH cells using reverse transcriptase-polymerase chain reaction; the cells expressed GluR1 and GluR4.²⁰ As previously described, these cell lines have the same profile as that of the primary glioblastoma cells de novo.

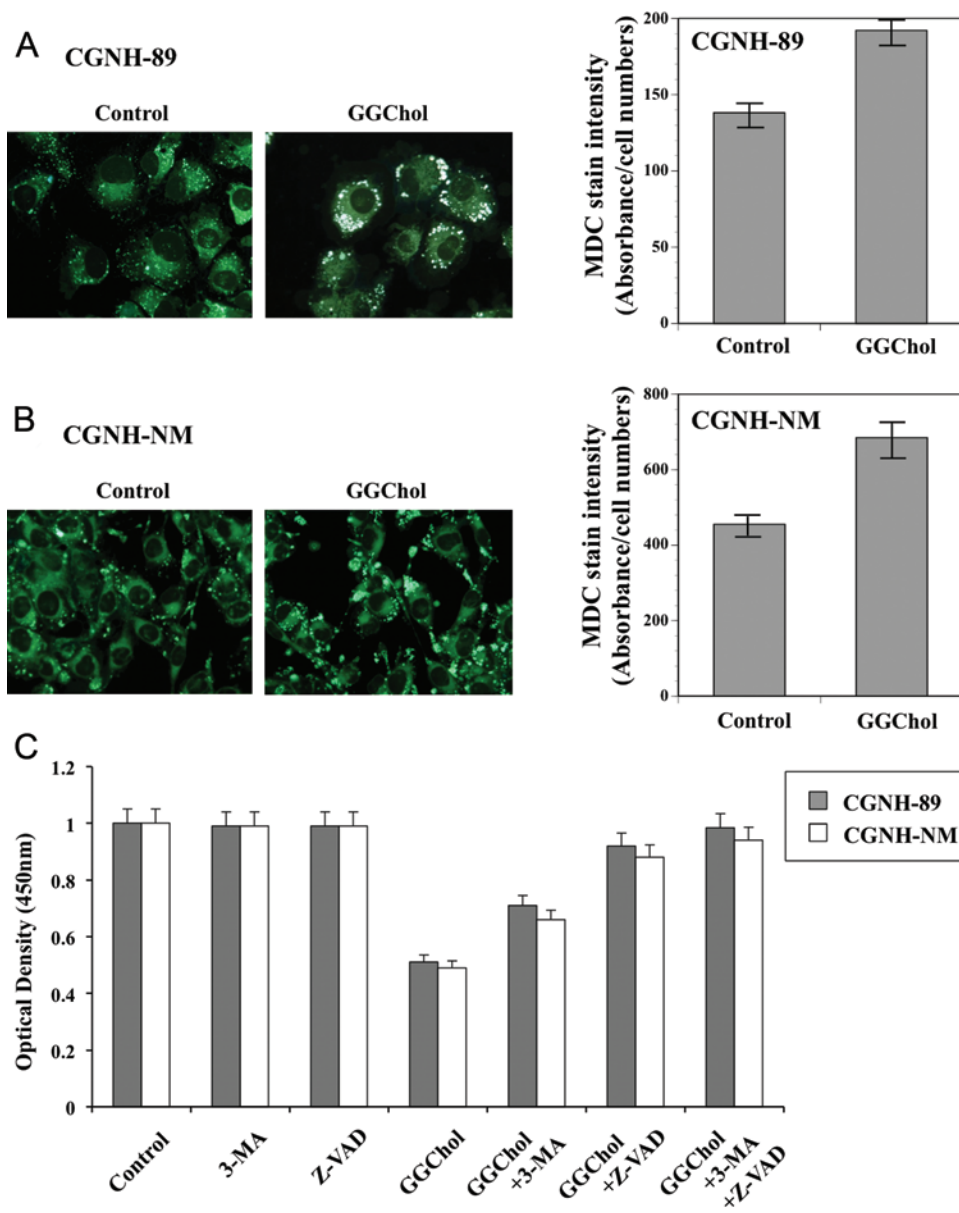


Fig. 4. Fluorescence microscope images showing induction of autophagic cell death in CGNH-89 (A) and CGNH-NM (B) cells. Original magnification $\times 200$. Bar graph (C) demonstrates cell viability in the glioblastoma cells treated with GGChol measured in the presence of antiapoptosis and antiautophagy reagents. Monodansylcadaverine incorporation was quantified and presented as the fold increase \pm SEM compared with the control (bar graph, upper right). The figures and values are from 3 independent experiments.

In glioblastoma cells treated with sugar cholestanols, the activation of the initiator caspases (extrinsic caspase-8 and intrinsic caspase-9) followed by the activation of the executor caspase (caspase-3) occurred in the glioblastoma cells after treatment with sugar cholestanols. Accordingly, the activation of the cascade involving such caspases induced PARP cleavage, resulting in nuclear fragmentation. Furthermore, the induction of the apoptosis signaling pathway in glioblastoma cells treated with sugar cholestanols appeared to suppress the expression of Bcl-xL and to enhance the expression of Bax in antiapoptotic and proapoptotic manners, respectively. Therefore, the induction of apoptosis appeared to be caused by the disruption of a

balance between these anti- and proapoptotic molecules, as described previously.^{8,14,15}

One of the most important survival-signaling pathways is mediated by PI3K and its downstream targets, such as Akt and mTOR.²⁹ Recently, Akt was reported to play an important role in determining the chemosensitivity of many types of cells.^{7,10,35} The induction of autophagy requires the activation of Beclin-1 and its interacting partner, Class III PI3K, resulting in the generation of phosphatidylinositol-3'phosphates. This induction is negatively regulated by Class I PI3K via the Akt/mTOR pathway.^{41,44,46} In contrast, Beclin-1, a mammalian homolog of the yeast autophagy-related gene Atg6, was observed to be

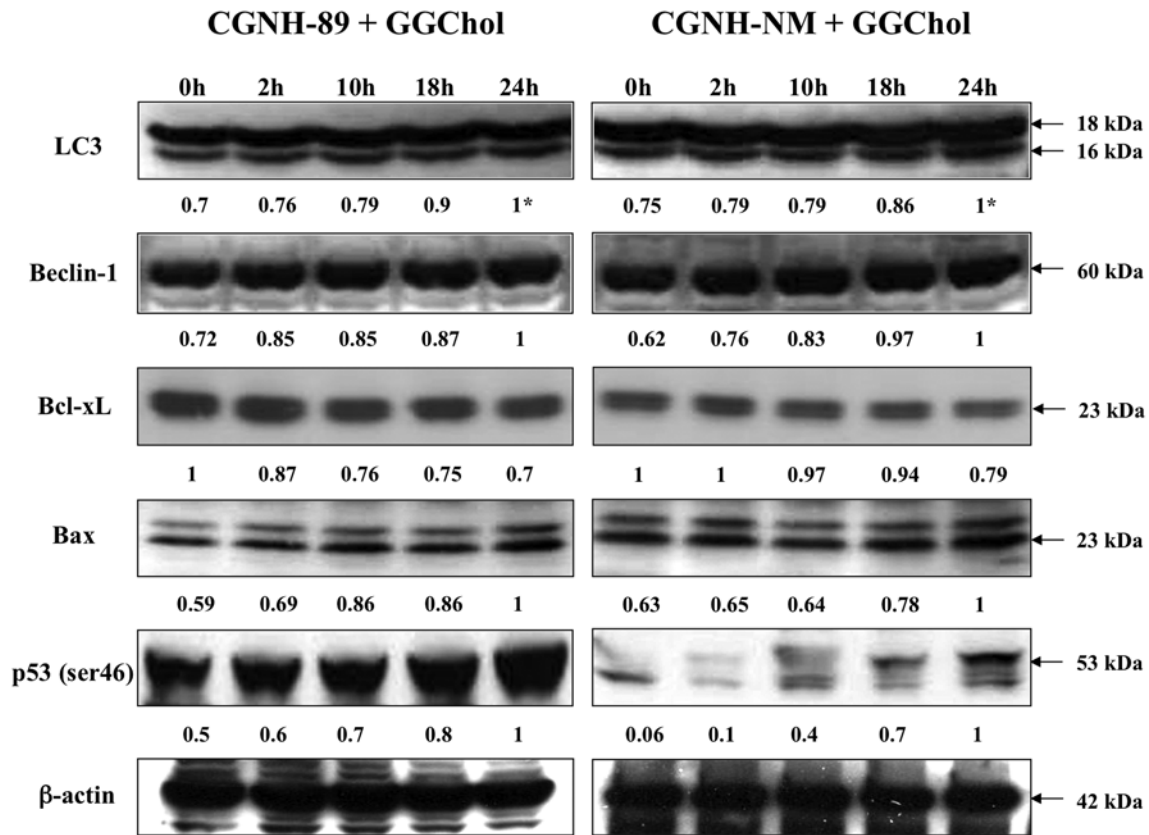


Fig. 5. Western blot analysis in the glioblastoma cells treated with GGChol. Changes in the expression of the autophagy activation, Bcl-2 family members, p53 (ser46) in the CGNH-89 and CGNH-NM cells are shown. The cells were treated with 30 μ M of GGChol for 24 hours, and values given below each figure indicate the calculation of each band, and the LC3 active form band (16 kDa), after normalization of their expression to that of β -actin, shown as a percentage compared with the control. There was a significant increase in the active form of LC3 (16 kDa) measured using densitometric analysis.

deleted in breast and prostate cancer cells, and its expression was shown to induce autophagy and inhibit tumorigenicity in MCF-7 breast cancer cells.²⁷ Furthermore, the microtubule associated protein 1 light chain 3, designated as LC3, exists in 2 forms, which are LC3-I and LC3-II, located in the cytosol and autophagosomal membranes, respectively. LC3 is the first protein that was reported to specifically localize to autophagosome membranes and was later designated as LC3-II (16 kDa), the inner limiting membrane of the autophagosome. During the process of autophagy, cleaved LC3-I conjugates with phosphatidylethanolamine to form LC3-II, which is an important step for autophagosome formation.²⁵ Immunofluorescence staining of endogenous LC3 can detect autophagy (Fig. 4). The expression of Beclin-1 in glioblastoma cells was slightly increased after treatment with sugar cholestanols along with the decreased expression of the members of the Akt/mTOR pathway. In addition, LC3-II expression was increased, and this hallmark could be used to estimate the abundance of autophagosomes before they are destroyed via fusion with lysosomes.

Recently, p53 has also been revealed to activate autophagy.²² Several groups have reported the localization of p53 to the outer layer of the mitochondrial membrane and the activation of apoptosis through direct binding to

the Bcl-2 family members Bax, Bak, or Bcl-xL.^{5,30} The overexpression of p53 was also reported to increase Bax expression in several cell types following the induction of apoptosis.^{31,43} The binding of p53 to p53AIP1, which appears to be important for the apoptotic response, is selectively enhanced by the phosphorylation of ser46.³⁷ We also observed that, in fact, p53 at ser46 was increased in glioblastoma cells after treatment with sugar cholestanols. In addition, the stimulation of cell death controlled by apoptosis and/or at least partially by autophagy was observed in glioblastoma cells treated with sugar cholestanols and cotreated with inhibitors of caspases and autophagy. Therefore, we provided evidence that sugar cholestanols induced apoptosis and autophagic cell death in the same glioblastoma cells. The occurrence of cell death induced by apoptosis was also observed in colorectal cancer cells treated with the same sugar cholestanols (S. Yazawa et al., unpublished observation, 2008).

The mechanism of drug-induced cell death has been accepted to be governed not only by the upregulation of proapoptotic, proautophagic factors or tumor suppressors, but also by the modulation of the survival-signaling pathways.¹¹ As we previously showed, CGNH cells express Ca²⁺-permeable AMPA receptors assembled mainly from the GluR1 and/or GluR4 subunits, which contribute to the

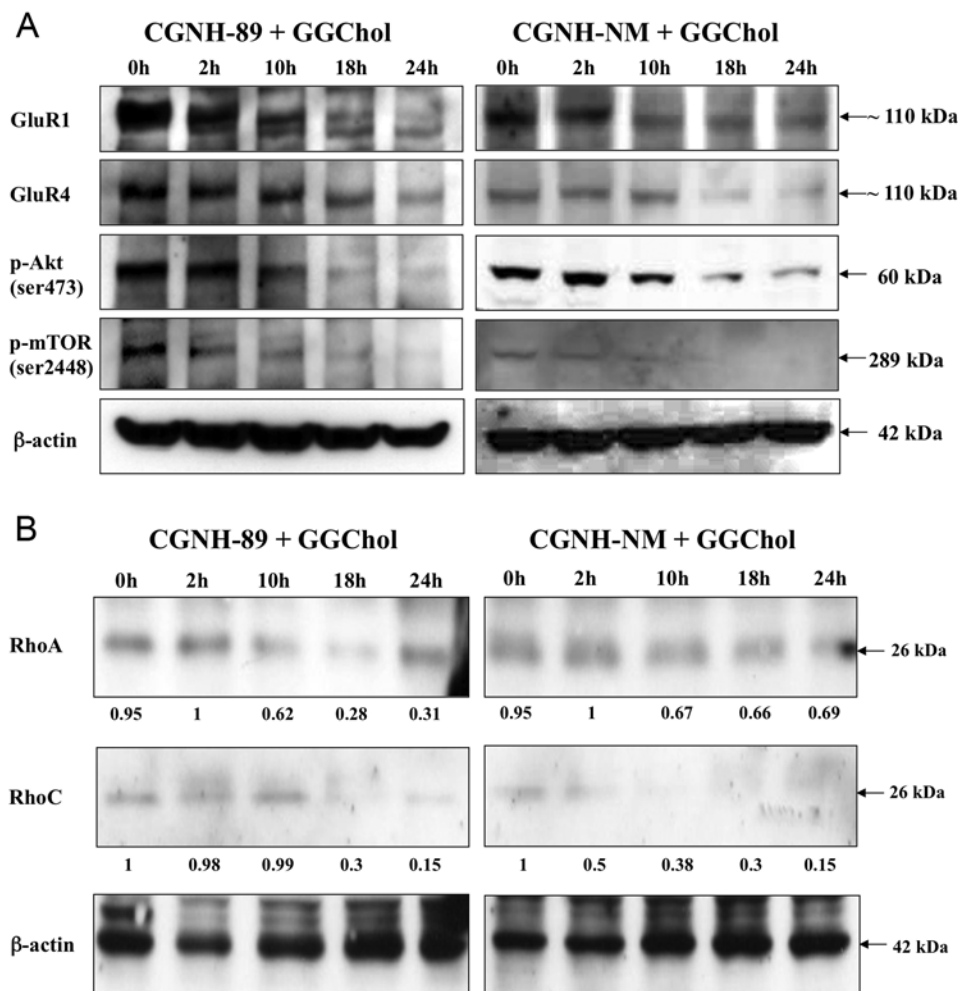


Fig. 6. Western blot analysis of glioblastoma cells treated with GGChol. Changes in the expression levels of the glutamate receptors (GluR1 and GluR4), p-Akt, and p-mTOR (**A**) and Rho GTPases (**B**) in the CGNH-89 and CGNH-NM cells are shown. The CGNH cells were treated with 30 μ M of GGChol for 24 hours. The values given below the Rho GTPase figures indicate the calculation of each band after normalization of the expression to that of β -actin, shown as a percentage compared with the control.

invasive and aggressive behavior of glioblastoma.²⁰ Cell growth appeared to be suppressed in cancer cells treated with the sugar cholestanols, particularly through the activation of the Akt/mTOR pathway (A. Faried et al., unpublished observation, 2009). As reported previously, there is an important survival-signaling pathway that is mediated by the Akt/mTOR pathway²⁹ and its upstream target, the AMPA receptors.²¹

Our results demonstrated that the sugar cholestanols inhibit the activation of the Akt/mTOR pathway, as shown by the downregulation of phosphorylated Akt at ser473 and phosphorylated mTOR at ser2448. Therefore, we analyzed the expression of the glutamate-AMPA receptors as an upstream target of Akt/mTOR in glioblastoma cells. As expected, we found that the sugar cholestanols inhibited the activation of the glutamate-AMPA receptors, GluR1 and GluR4, in both glioblastoma cell types tested. Taken together, our results suggest that the activation of the glutamate-AMPA receptors–Akt/mTOR pathway was downregulated after treatment with sugar cholestanols.

Ca²⁺-permeable AMPA receptors and Rho GTPase

family members facilitate the migration ability of human glioblastomas.^{20,47} In addition, we also evaluated the expression of Rho GTPases (RhoA and RhoC) because they were reported to be related to the degree of malignancy in glioblastoma.^{28,47} Furthermore, the inhibition of Rho GTPase signaling has been reported to decrease glioblastoma cell migration.²⁸ In this study, we showed that the expression of both RhoA and RhoC was decreased after treatment with the sugar cholestanols in a time-dependent manner. Overall, our results showed that different processes of cell death were induced by the sugar cholestanols and that the survival, proliferation, or metastatic properties of glioblastoma cells were affected by some other oncogenic factors (Fig. 8).

Our *in vivo* experiment using nude mice showed that the sugar cholestanols suppressed tumor growth of CGNH-89 cells that were injected into subcutaneous tissue, possessing the features of human glioblastomas in terms of histological tissue organization. This experiment may provide a reliable *in vivo* model for studying the response of human glioblastomas to our potential synthetic

Cell death of glioblastoma induced by glycans

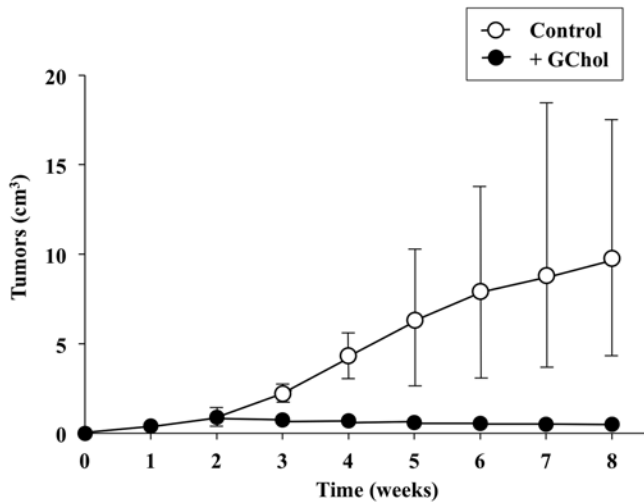


Fig. 7. Line graph showing the anticancer effect of sugar cholestanols on the subcutaneously formed tumors with glioblastoma cells. CGNH-89 cells (2×10^7 cells) were subcutaneously injected into nude mice. Injections of 120 μ l of GChol or phosphate-buffered saline only (as a control) were administered intratumorally 3 times (at 14, 15, and 16 days). The values of tumor volumes given indicate the mean \pm SD of 5 mice in each group.

glycans (sugar cholestanols). The sugar cholestanol injections reduced the incidence of intratumoral bleeding in the treated mice compared with the untreated mice, accompanied by the suppression of tumor growth and induction of apoptosis. These results indicate that programmed cell death controlled by apoptosis and/or at least partially by autophagy in CGNH cells was stimulated by treatment with our novel synthetic glycans (sugar cholestanols). It remains to be seen whether the sugar cholestanols could be applicable to an *in vivo* experiment using an intracranial glioma model to investigate their usefulness in chemotherapy against the expected blood-brain barrier.

Conclusions

The activation of programmed cell death in human malignant brain tumor cells induced by treatment with the sugar cholestanols may be involved in not only apoptosis, as we previously demonstrated in several tumor cell lines, but also autophagy, which was demonstrated here for the first time. The sugar cholestanols represent potential pharmaceutical agents against glioblastoma cells.

Disclosure

This work was supported partly by the 21st Century COE

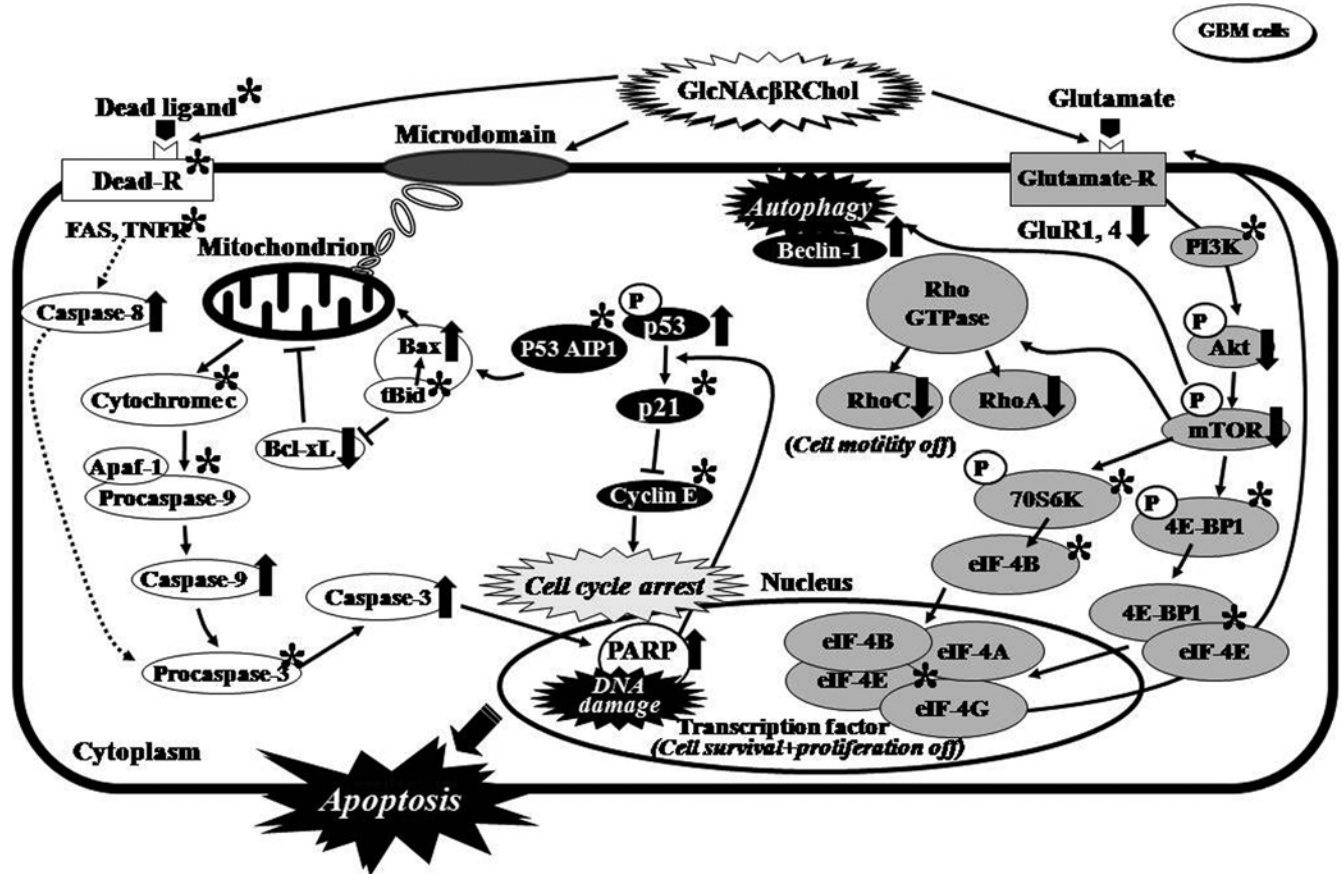


Fig. 8. The predicted effects of sugar cholestanols on cell death inducing both apoptosis and autophagy in the glioblastoma cells resulting from continuous activations and/or suppressions in the expressions of their related molecules. Molecules flagged with an asterisk were not examined in this study, but their details have been described in our previous studies.^{8-10,14,15,21} TNFR = tumor necrosis factor receptor.

Program, Japan; the Japan Society for the Promotion of Science; and a research grant for collaboration research to Dr. Faried from the Faculty of Medicine at Universitas Padjadjaran.

Author contributions to the study and manuscript preparation include the following. Conception and design: Faried, Arifin, Yazawa. Acquisition of data: Faried, Yazawa. Analysis and interpretation of data: Faried, Yazawa. Drafting the article: Faried, Yazawa. Critically revising the article: all authors. Reviewed submitted version of manuscript: all authors. Approved the final version of the manuscript on behalf of all authors: Faried.

References

- Biederbick A, Kern HF, Elsässer HP: Monodansylcadaverine (MDC) is a specific in vivo marker for autophagic vacuoles. **Eur J Cell Biol** **66**:3–14, 1995
- Bower M, Newlands ES, Bleeher NM, Brada M, Begent RJ, Calvert H, et al: Multicentre CRC phase II trial of temozolomide in recurrent or progressive high-grade glioma. **Cancer Chemother Pharmacol** **40**:484–488, 1997
- Bursch W, Ellinger A, Gerner C, Fröhwein U, Schulte-Hermann R: Programmed cell death (PCD). Apoptosis, autophagic PCD, or others? **Ann N Y Acad Sci** **926**:1–12, 2000
- Chamberlain MC, Kormanik PA: Practical guidelines for the treatment of malignant gliomas. **West J Med** **168**:114–120, 1998
- Chipuk JE, Kuwana T, Bouchier-Hayes L, Droin NM, Newmeyer DD, Schuler MM, et al: Direct activation of Bax by p53 mediates mitochondrial membrane permeabilization and apoptosis. **Science** **303**:1010–1014, 2004
- Edinger AL, Thompson CB: Death by design: apoptosis, necrosis and autophagy. **Curr Opin Cell Biol** **16**:663–669, 2004
- Fahy BN, Schlieman MG, Virudachalam S, Bold RJ: Inhibition of AKT abrogates chemotherapy-induced NF-kappaB survival mechanisms: implications for therapy in pancreatic cancer. **J Am Coll Surg** **198**:591–599, 2004
- Faried A, Faried LS, Nakagawa T, Yamauchi T, Kitani M, Sasabe H, et al: Chemically synthesized sugar-cholestanols possess a preferential anticancer activity involving promising therapeutic potential against human esophageal cancer. **Cancer Sci** **98**:1358–1367, 2007
- Faried A, Faried LS, Usman N, Kato H, Kuwano H: Clinical and prognostic significance of RhoA and RhoC gene expression in esophageal squamous cell carcinoma. **Ann Surg Oncol** **14**:3593–3601, 2007
- Faried LS, Faried A, Kanuma T, Nakazato T, Tamura T, Kuwano H, et al: Inhibition of the mammalian target of rapamycin (mTOR) by rapamycin increases chemosensitivity of CaSki cells to paclitaxel. **Eur J Cancer** **42**:934–947, 2006
- Fraser M, Leung B, Jahani-Asl A, Yan X, Thompson WE, Tsang BK: Chemoresistance in human ovarian cancer: the role of apoptotic regulators. **Reprod Biol Endocrinol** **1**:66, 2003
- Fritz G, Just I, Kaina B: Rho GTPases are over-expressed in human tumors. **Int J Cancer** **81**:682–687, 1999
- Goto J, Suzaki K, Nambara T: Synthesis of conjugated cholesterol and cholestanols. **Chem Pharm Bull (Tokyo)** **27**:1926–1931, 1979
- Hashimoto S, Tsuboi K, Asao T, Kuwano H, Nishimura T, Nakagawa T, et al: Anti-tumor effect of chemically synthesized novel glycoconjugates. **Glycoconj J** **22**:311, 2005
- Hahimoto S, Yazawa S, Asao T, Faried A, Nishimura T, Tsuboi K, et al: Novel sugar-cholestanols as anticancer agents against peritoneal dissemination of tumor cells. **Glycoconj J** **25**:531–544, 2008
- Hoelzinger DB, Mariani L, Weis J, Woyke T, Berens TJ, McDonough WS, et al: Gene expression profile of glioblastoma multiforme invasive phenotype points to new therapeutic targets. **Neoplasia** **7**:7–16, 2005
- Hoorens A, Van de Castele M, Klöppel G, Pipeleers D: Glucose promotes survival of rat pancreatic beta cells by activating synthesis of proteins which suppress a constitutive apoptotic program. **J Clin Invest** **98**:1568–1574, 1996
- Horiuchi A, Imai T, Wang C, Ohira S, Feng Y, Nikaido T, et al: Up-regulation of small GTPases, RhoA and RhoC, is associated with tumor progression in ovarian carcinoma. **Lab Invest** **83**:861–870, 2003
- Ishiuchi S, Nakazato Y, Iino M, Ozawa S, Tamura M, Ohye C: In vitro neuronal and glial production and differentiation of human central neurocytoma cells. **J Neurosci Res** **51**:526–535, 1998
- Ishiuchi S, Tsuzuki K, Yoshida Y, Yamada N, Hagimura N, Okado H, et al: Blockage of Ca²⁺-permeable AMPA receptors suppresses migration and induces apoptosis in human glioblastoma cells. **Nat Med** **8**:971–978, 2002
- Ishiuchi S, Yoshida Y, Sugawara K, Aihara M, Ohtani T, Watanabe T, et al: Ca²⁺-permeable AMPA receptors regulate growth of human glioblastoma via Akt activation. **J Neurosci** **27**:7987–8001, 2007
- Jin S: p53, autophagy and tumor suppression. **Autophagy** **1**:171–173, 2005
- Kamai T, Tsujii T, Arai K, Takagi K, Asami H, Ito Y, et al: Significant association of Rho/ROCK pathway with invasion and metastasis of bladder cancer. **Clin Cancer Res** **9**:2632–2641, 2003
- Kanzawa T, Germano IM, Komata T, Ito H, Kondo Y, Kondo S: Role of autophagy in temozolomide-induced cytotoxicity for malignant glioma cells. **Cell Death Differ** **11**:448–457, 2004
- Kondo Y, Kanzawa T, Sawaya R, Kondo S: The role of autophagy in cancer development and response to therapy. **Nat Rev Cancer** **5**:726–734, 2005
- Lefranc F, Brotchi J, Kiss R: Possible future issues in the treatment of glioblastomas: special emphasis on cell migration and the resistance of migrating glioblastoma cells to apoptosis. **J Clin Oncol** **23**:2411–2422, 2005
- Liang XH, Jackson S, Seaman M, Brown K, Kempkes B, Hibshoosh H, et al: Induction of autophagy and inhibition of tumorigenesis by beclin 1. **Nature** **402**:672–676, 1999
- Manning TJ Jr, Parker JC, Sontheimer H: Role of lysophosphatidic acid and rho in glioma cell motility. **Cell Motil Cytoskeleton** **45**:185–199, 2000
- McCormick F: Cancer: survival pathways meet their end. **Nature** **428**:267–269, 2004
- Mihara M, Erster S, Zaika A, Petrenko O, Chittenden T, Pancoska P, et al: p53 has a direct apoptogenic role at the mitochondria. **Mol Cell** **11**:577–590, 2003
- Miyashita T, Krajewski S, Krajewska M, Wang HG, Lin HK, Liebermann DA, et al: Tumor suppressor p53 is a regulator of bcl-2 and bax gene expression in vitro and in vivo. **Oncogene** **9**:1799–1805, 1994
- Munafó DB, Colombo MI: A novel assay to study autophagy: regulation of autophagosome vacuole size by amino acid deprivation. **J Cell Sci** **114**:3619–3629, 2001
- Nelson DA, White E: Exploiting different ways to die. **Genes Dev** **18**:1223–1226, 2004
- Newton HB: Small-molecule and antibody approaches to molecular chemotherapy of primary brain tumors. **Curr Opin Investig Drugs** **8**:1009–1021, 2007
- Nguyen DM, Chen GA, Reddy R, Tsai W, Schrupp WD, Cole G Jr, et al: Potentiation of paclitaxel cytotoxicity in lung and esophageal cancer cells by pharmacologic inhibition of the phosphoinositide 3-kinase/protein kinase B (Akt)-mediated signaling pathway. **J Thorac Cardiovasc Surg** **127**:365–375, 2004
- Nichols WW, Murphy DG, Cristofalo VJ, Toji LH, Greene AE, Dwight SA: Characterization of a new human diploid cell strain, IMR-90. **Science** **196**:60–63, 1977
- Oda K, Arakawa H, Tanaka T, Matsuda K, Tanikawa C, Mori T, et al: p53AIP1, a potential mediator of p53-dependent apop-

Cell death of glioblastoma induced by glycans

- tosis, and its regulation by Ser-46-phosphorylated p53. **Cell** **102**:849–862, 2000
38. Ogier-Denis E, Codogno P: Autophagy: a barrier or an adaptive response to cancer. **Biochim Biophys Acta** **1603**:113–128, 2003
 39. Osaki M, Oshimura M, Ito H: PI3K-Akt pathway: its functions and alterations in human cancer. **Apoptosis** **9**:667–676, 2004
 40. Paglin S, Hollister T, Delohery T, Hackett N, McMahon M, Sphicas E, et al: A novel response of cancer cells to radiation involves autophagy and formation of acidic vesicles. **Cancer Res** **61**:439–444, 2001
 41. Petiot A, Ogier-Denis E, Blommaert EF, Meijer AJ, Codogno P: Distinct classes of phosphatidylinositol 3'-kinases are involved in signaling pathways that control macroautophagy in HT-29 cells. **J Biol Chem** **275**:992–998, 2000
 42. Sasaki A, Tamura M, Hasegawa M, Ishiuchi S, Hirato J, Nakazato Y: Expression of interleukin-1beta mRNA and protein in human gliomas assessed by RT-PCR and immunohistochemistry. **J Neuropathol Exp Neurol** **57**:653–663, 1998
 43. Selvakumaran M, Lin HK, Miyashita T, Wang HG, Krajewski S, Reed JC, et al: Immediate early up-regulation of bax expression by p53 but not TGF beta 1: a paradigm for distinct apoptotic pathways. **Oncogene** **9**:1791–1798, 1994
 44. Shintani T, Klionsky DJ: Autophagy in health and disease: a double-edged sword. **Science** **306**:990–995, 2004
 45. Stupp R, Mason WP, van den Bent MJ, Weller M, Fisher B, Taphoorn MJ, et al: Radiotherapy plus concomitant and adjuvant temozolomide for glioblastoma. **N Engl J Med** **352**:987–996, 2005
 46. Wang CW, Klionsky DJ: The molecular mechanism of autophagy. **Mol Med** **9**:65–76, 2003
 47. Yan B, Chour HH, Peh BK, Lim C, Salto-Tellez M: RhoA protein expression correlates positively with degree of malignancy in astrocytomas. **Neurosci Lett** **407**:124–126, 2006
 48. Yung WK, Prados MD, Yaya-Tur R, Rosenfeld SS, Brada M, Friedman HS, et al: Multicenter phase II trial of temozolomide in patients with anaplastic astrocytoma or anaplastic oligoastrocytoma at first relapse. **J Clin Oncol** **17**:2762–2771, 1999

Manuscript submitted July 16, 2013.

Accepted January 23, 2014.

Please include this information when citing this paper: published online March 28, 2014; DOI: 10.3171/2014.1.JNS131534.

Address correspondence to: Ahmad Faried, M.D., Ph.D., Department of Neurosurgery, Faculty of Medicine, Universitas Padjadjaran–Dr. Hasan Sadikin Hospital, Jl. Pasteur No. 38, Bandung, West Java 40161, Indonesia. email: faried.fkup@gmail.com.

神経膠芽腫に対する Akt を標的とした分子標的療法

渡邊 孝, 菅原健一, 長嶺英樹, 石内勝吾

琉球大学医学部 脳神経外科

Targeted Molecular Therapy Against the Multiple Akt-mediated Signaling Pathways in Glioblastoma

Takashi Watanabe, MD, Phd., Kenichi Sugawara, MD, PhD
Hideki Nagamine, MD and Shogo Ishiuchi, MD, PhD

*Department of Neurosurgery, Graduate School of Medicine,
University of the Ryukyus, Okinawa, Japan*

ABSTRACT

Glioblastoma multiforme is the most malignant tumor occurring in the central nervous system and is incurable by current therapeutic strategies. The serine/threonine-specific protein kinase, Akt, is frequently dysregulated and affects cell survival and proliferation in many human cancers, including glioblastoma. Inhibition of Akt phosphorylation has demonstrated therapeutic potential against glioblastoma. Many inhibitors of the PI3K-Akt signaling pathway and α -amino-3-hydroxy-5-methyl-4-isoxazolepropionate (AMPA)-Akt signaling pathway are in clinical use and have demonstrated preliminary activity against various tumor types. This review describes the limitations of therapy against glioblastoma targeting single dysregulated pathways because of the presence of diverse signaling pathways that regulate the coactivation of multiple tyrosine kinases in most malignant gliomas, and the requirement for combined approaches targeting the multiple Akt-mediated signaling pathways based on the findings of clinical trials and earlier investigations. *Ryukyu Med. J., 33 (1~3) 1~8, 2014*

Key words: AMPA, Akt, glioblastoma, PI3K, platelet-derived growth factor

はじめに

神経膠芽腫は、中枢神経系で最も悪性度が高く、予後不良な疾患である。極めて高い増殖能と浸潤能により、開頭術で完全に摘出することが困難であるため、放射線治療、化学療法を組み合わせた集学的治療が必要であるが、現在の標準治療では治癒困難である¹⁻³⁾。

拡大局所放射線治療 (60Gy/30Fr) と Temozolomide (TMZ) 75mg/m²・42 間投与を行った後、TMZ 150-200mg/m²・5 日間を 28 日周期で投与し、6 周期投与する治療法 (Stupp regimen) を用いた第三相臨

床試験において、全生存期間中央値 (median overall survival: mOS) が放射線治療単独の 12.1 ヶ月と比較し、放射線治療・TMZ 併用投与で 14.6 ヶ月と有意な延長を示した。このことから、この regimen が、現在の神経膠芽腫に対する標準的治療法となっているが、2 年生存率 27.2% 及び 5 年生存率 9.8% と低率であり、依然として十分な効果が得られていないのが現状である²⁾。

その後の研究で、DNA 修復酵素である O6-methylguanine-DNA methyltransferase (MGMT) の発現率が高いと、TMZ の効果が減弱することが判明した⁴⁾。これに対し、Interferon (INF)- β が、腫瘍抑制

遺伝子である p53 を介して MGMT の発現を抑制する効果を有することが示された⁵⁾。Stupp regimen に INF- β 300 万単位を併用投与した臨床試験 (INTEGRA study) が本邦において行われ、明らかな有害事象の増加がなく、mOS が 17.1 ヶ月と延長し、12 ヶ月の無増悪生存期間 (progression free survival: PFS) が 50% と治療効果の改善がみられた⁶⁾。

本邦でも、2013 年より Bevacizumab (アバスタン[®]) が悪性神経膠腫に対して保険適応となった。初発神経膠芽腫に対する bevacizumab の効果を検証する大規模第三相試験 (AVA glio 試験と、RTOG 0825 試験) は、標準治療 (Stupp regimen) に Bevacizumab を追加投与し、プラセボと比較した二重盲検無作為化比較検討試験である。その結果において、PFS は、bevacizumab 投与群で AVA glio 試験 10.6 ヶ月、RTOG 0825 試験 10.7 ヶ月であり、プラセボ群と比較して 3-4 ヶ月延長したが、mOS は、Bevacizumab 投与群で、AVA glio 試験 16.8 ヶ月、RTOG 0825 試験 15.7 ヶ月であり、どちらもプラセボ群と比べて有意な延長効果は得られなかった^{7,8)}。

以上のように、現在本邦で、神経膠芽腫、悪性神経膠腫に対して主に用いられている化学療法薬は、TMZ (INF- β 併用) と Bevacizumab であり、これまでの治療法の進歩により、OS, PFS の延長が認められてきたが、mOS は、15-17 ヶ月と限定的であった。このため、新たな治療薬や治療方法の開発が切望されており、その中で分子標的療法が注目されている。複数のシグナル伝達経路の中で、Akt を介するシグナル伝達経路が重要視されてきており、他の固形癌に対しても、このシグナル伝達経路を標的とした治療法が盛んに開発されている。本稿では、認容性が良好で、様々な悪性腫瘍に対して臨床的に使用可能となっている Akt を標的とした分子標的療法の神経膠芽腫に対する臨床応用について概説する。

Akt を介する分子標的療法

Akt は、Plekstrin Homology (PH) ドメインを有するセリン/スレオニンキナーゼであり、腫瘍細胞の生存、増殖、分化、遊走、血管新生において重要な役割を果たしている。近年の研究から、神経膠芽腫の生存、増殖、遊走、血管新生に Akt の活性化が関与していることが判明し、治療の標的として注目を集めてきた^{3,9-15)}。Akt は、PI3K-Akt シグナル伝達経路の中心に位置し、Thr-308 と Ser-473 でリン酸化されて活性化され、抗アポトーシス活性による腫瘍細胞の生存や増殖に関与するといわれている^{11,16-21)}。神経膠芽腫細胞では、epidermal growth factor receptor (EGFR), platelet-derived growth factor receptor (PDG-

FR) といったチロシンキナーゼ受容体の増幅による PI3K-Akt シグナル伝達経路の活性化が認められている²²⁻²⁶⁾。また、神経膠芽腫には vascular endothelial growth factor (VEGF) が過剰発現し、腫瘍の血管新生や悪性度、予後に関与しており、VEGF に対する抗体が神経膠芽腫の腫瘍形成を抑制することが判明している²⁷⁾。神経膠芽腫細胞は、主に GluR1 と GluR4 サブユニットで構成されるカルシウム透過型 α -amino-3-hydroxy-5-methyl-4-isoxazolepropionate (AMPA) 型グルタミン酸受容体を発現している^{28,29)}。この受容体を介する細胞内カルシウム濃度の上昇による Ser-473 での Akt のリン酸化が神経膠芽腫の増殖、浸潤に関与することが解明され、このシグナル伝達経路は、PI3K-Akt シグナル伝達経路とは独立していることが判明した^{9,30)}。Phosphatase and tensin homolog Deleted from Chromosome 10 (PTEN) を欠失した神経膠芽腫では、Sonic Hedgehog (shh) シグナル伝達経路が活性化され、p70 S6 kinase (S6K) の活性化を介して、腫瘍細胞の生存や増殖に関与していることが明らかとなっている³¹⁾。

神経膠芽腫は、腫瘍増殖や血管新生に関する複数のシグナル伝達経路を有し、相互に活性化していることが知られており、単剤での抗腫瘍効果が制限される原因と考えられている^{3,32)}。このため、複数のシグナル伝達経路を抑制する多剤併用療法が重要視されている³²⁾。Akt を中心としたシグナル伝達経路も複数存在し、相互に密接に関連しているため、複数のシグナル伝達経路を標的とした多剤併用分子標的療法が必要と考えられる (Fig 1)。近年、これらのシグナル伝達経路を標的とした分子標的薬が次々に開発され、様々な固形癌に対する臨床試験が行われて実用化されている。認容性が良好である分子標的療法薬は、将来的に神経膠芽腫に臨床応用が可能となる可能性があり、これらの効果を検証する研究が重要である。

臨床試験における単剤投与の限界

AMPA 受容体拮抗薬

カルシウム透過型 AMPA 受容体拮抗薬である 2,3-dihydroxy-6-nitro-7-sulfamoyl-benzo-(F)-quinoxaline (NBQX) は、Ser-473 での Akt のリン酸化を抑制し、神経膠芽腫細胞株の増殖と遊走を抑制することが判明している。しかし、NBQX は、静脈内投与を行うと腎尿細管で凝結するため現実的ではない。[2,3-dioxo-7-(1H-imidazol-1-yl)-6-nitro-1,2,3,4-tetrahydroquinoxalin-1-yl]-acetic acid monohydrate (YM872) は、経口摂取が可能であり、水に溶解性であり、生体に投与するという点では現実的である³³⁾。Talampanel は、認容性が良好で、経口摂取が可能で、

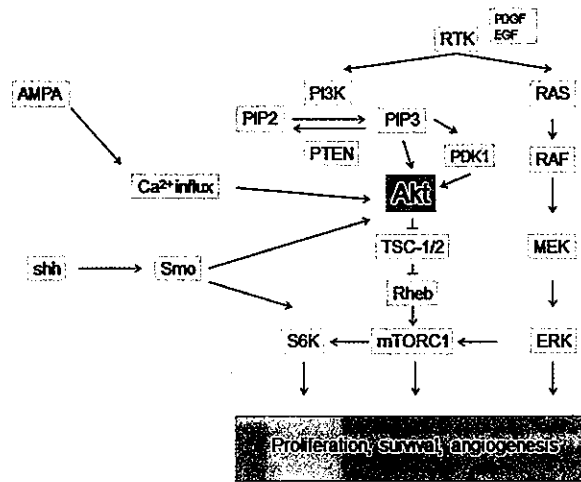


Fig. 1 Schematic representation of the Akt signaling pathway and its main components

EGF, epidermal growth factor; PDGF, platelet-derived growth factor; RTK, receptor tyrosine kinase; RAS, rat sarcoma oncogene; RAF, murine sarcoma viral oncogene; MEK, mitogen-activated protein; ERK, extracellular signal-related kinase; mTORC1, mammalian target of rapamycin complex 1; PI3K, phosphatidylinositol 3-kinase; PIP2, phosphatidylinositol 4,5-bisphosphate; PIP3, phosphatidylinositol 3,4,5-trisphosphate; PDK1, 3-phosphoinositide dependent protein kinase-1; PTEN, phosphatase and tensin homolog; TSC-1/2, tuberous sclerosis complex-1/2; Rheb, RAS homologue enriched in brain; S6K, S6 kinase; AMPA, α -amino-3-hydroxy-5-methyl-4-isoxazolepropionate; shh, sonic hedgehog; Smo, smoothened.

非競合性のカルシウム透過型 AMPA 受容体拮抗薬で、中枢神経への移行性も優れている薬剤であり、臨床試験で使用されている³⁴⁾。多施設共同研究による第二相臨床試験では、新規神経膠芽腫症例(年齢 18 歳から 70 歳)60 例に対して、Stupp regimen に talampanel (25mg × 3 / 日から 75mg × 3 / 日へ 1 週間ごとに増量)を連日併用投与した結果、mOS 20.3 ヶ月、2 年生存率 41.7% であり、Stupp regimen による標準治療の結果 (mOS 14.6 ヶ月、2 年生存期間 26.5%) と比較して、有害事象を増加させることなく、生存期間を延長させた³⁵⁾。しかし、再発悪性神経膠腫(神経膠芽腫 22 例、退形成性神経膠腫 8 例)に対し、talampanel(25-75mg × 3 / 日)を連日単剤投与した第二相臨床試験では、partial response が膠芽腫 1 例(5%)のみであり、6 ヶ月の PFS は、膠芽腫 4.6%、退形成性神経膠腫 0%、median PFS は、膠芽腫 5.9 週、退形成性神経膠腫 8.9 週であった。倦怠感、めまい、失調といった有害事象は軽度であったが、有意な抗腫瘍効果を認めておらず、多数のシグナル伝達経路を有する悪性神経膠腫に対する単剤投与での治療の困難さを示している³⁶⁾。

PDGF 受容体拮抗薬

メシル酸イマチニブ (Imatinib mesylate) は、Bcl-

Abl, PDGF α 受容体, PDGF β 受容体, c-kit チロシンキナーゼ活性を阻害する抗腫瘍薬である。慢性骨髄性白血病と消化管間質腫瘍で臨床的に使用されており³⁷⁻³⁹⁾、神経膠芽腫に対する治療薬としても期待された。しかし、55 例の再発悪性神経膠芽腫(膠芽腫 34 例、退形成性神経膠腫 21 例)に対してメシル酸イマチニブ 600 ~ 800mg / 日を単剤投与した第二相臨床試験では、6 ヶ月 PFS は、膠芽腫 3%、退形成性神経膠腫 10% であり、5 例で腫瘍内出血が認められた⁴⁰⁾。また、112 例の再発悪性神経膠芽腫(膠芽腫 51 例、退形成性星細胞腫 25 例、退形成性乏突起膠腫 36 例)に対してメシル酸イマチニブ 600 ~ 800mg / 日を単剤投与した第二相臨床試験では、6 ヶ月 PFS は、膠芽腫 16%、退形成性星細胞腫 9%、退形成性乏突起膠腫 4% であり、いずれの臨床試験においても単剤投与の効果は低く限定的であるという結果に終わった。

抗 VEGF 受容体抗体

再発膠芽腫に対する bevacizumab 単剤投与(10mg/kg, 2 ~ 3 週間毎)を行った第二相臨床試験では、Bevacizumab 投与により、脳浮腫の軽減とステロイド投与量を減量できるという点が有利であったが、6 ヶ月の PFS:25-42.6%, median PFS: 2.7 ~ 4.2 ヶ月、mOS:6.4 ~ 10.5 ヶ月であり、Bevacizumab の単独

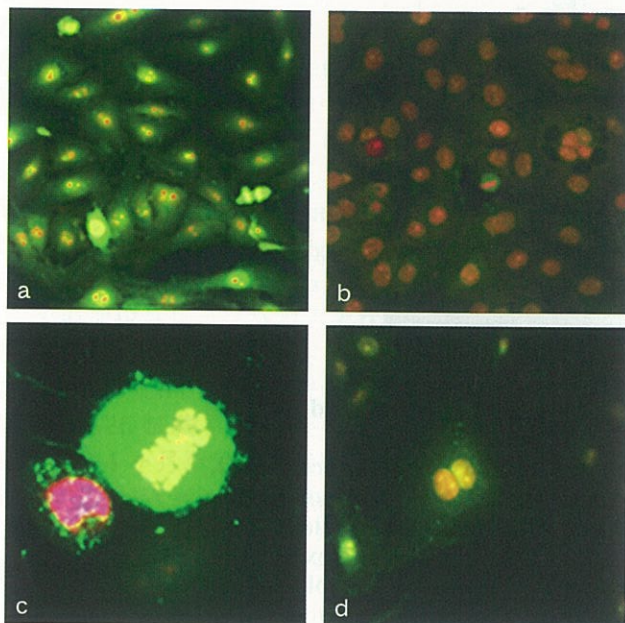


Fig. 2

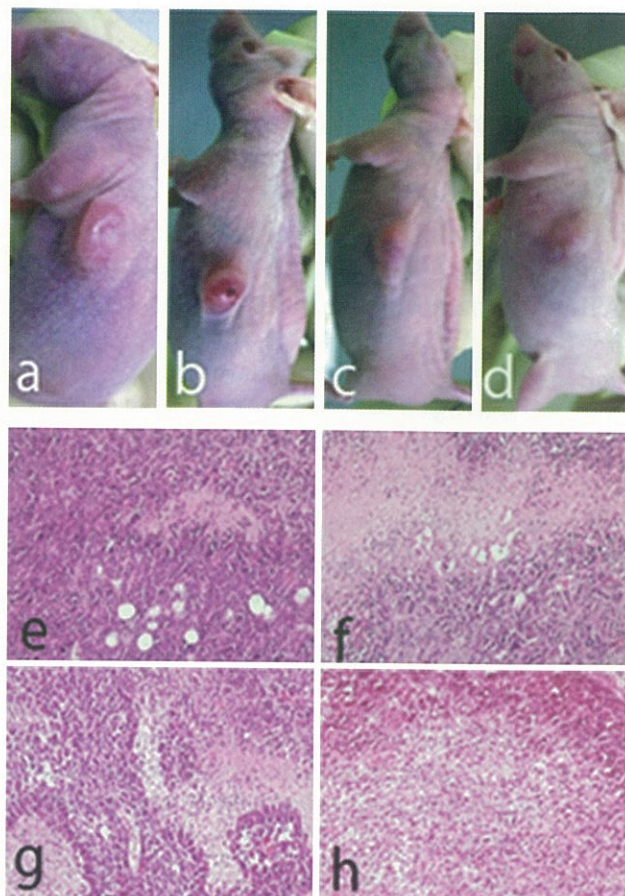


Fig. 3

Fig. 2 Effect of combination therapy targeting the AMPA-Akt signaling pathway and PI3K-Akt signaling pathway in vitro

Human glioblastoma cells were treated with PBS (control; left column), or calcium-permeable AMPA receptor antagonist (YM872 at 20 μ M) and PDGF receptor antagonist (AG1296 at 20 μ M) (right column). Immunofluorescence staining is shown for phosphorylated Akt in green, for Ki-67 in blue, and for propidium iodide in red.

Fig. 3 Effect of combination therapy targeting the AMPA-Akt signaling pathway and PI3K-Akt signaling pathway in vivo

a-d: Glioblastoma cell suspensions were injected subcutaneously into the flank of nude mice. Inhibition of tumor growth was observed after daily intraperitoneal injection of PBS (control; a), calcium-permeable AMPA receptor antagonist (YM872 at 25 mg/kg; b), PDGF receptor antagonist (AG1296 at 1.25 mg/kg; c), or the combination of both antagonists (d) for 2 weeks.

e-h: Photomicrographs of sections of tumor tissue taken 36 days after inoculation, treated with PBS (e), 25 mg/kg YM872 (f), 1.25 mg/kg AG1296 (g), and the combination of both agents (h). Extensive necrosis in the tumor tissue was found after treatment with YM872, AG1296, and the combination of both agents. Hematoxylin and eosin stain, original magnification: $\times 200$.

投与による効果は限定的であった⁴¹⁻⁴³). これまで臨床試験で使用されてきた悪性神経膠腫に対する分子標的治療薬は、認容性は良好であったが、単剤投与での効果はどれも限定的なものであった。

多剤併用化学療法の効果

AMPA-Akt シグナル伝達経路と PI3K-Akt シグナル伝達経路の両シグナル伝達経路を標的とし

た我々の最新の研究において、神経膠芽腫細胞株 (CGNH-89, U87, HKG) にカルシウム透過型 AMPA 受容体拮抗薬である YM872 と PDGF 受容体拮抗薬である AG1296 を併用投与した場合、AG1296 投与群、YM872 投与群と併用投与群では、control と比較し、腫瘍増殖及び Akt のリン酸化ともに有意に抑制された。この効果は正常マウス海馬神経細胞では認められず、正常神経細胞を阻害することなく、腫瘍増殖を抑

制することが判明した (Fig 2). In vitro では, この抑制効果には, 単独投与と併用投与の間での有意差が認められなかったが, ヒト神経膠芽腫をヌードマウスに移植した異種移植モデルを用いた解析では, control と比較し, AG1296 投与群, YM872 投与群, 併用群で腫瘍体積の減少, 壊死巣の増加及び細胞密度の減少が認められた (Fig.3). また, Ki-67 標識率及び CD34 で標識した腫瘍血管数は, 各治療群で有意に減少し, 併用投与における相乗効果が認められた. このことから, 異種移植モデルにおいて併用投与群の抗腫瘍効果が増強したのは, vascular niche の抑制によるものと考えられた⁴⁴⁾. PDGF 受容体拮抗薬である Imatinib mesylate や AMPA 受容体拮抗薬である Talampanel は, 単独投与での効果は限定的であるが, 併用投与による効果が期待される. また, PTEN が欠失して PI3K シグナル伝達経路が活性化された神経膠芽腫細胞に, 経口 PI3K 阻害薬である BKM120(Buparlisib) と Smoothed (Smo) の阻害薬で Sonic Hedgehog (shh) シグナル伝達経路を抑制する LDE225 (sonidegib) を併用投与した最近の研究では, 併用投与により腫瘍の増殖抑制とアポトーシス誘導に相乗効果が認められた³¹⁾. BKM120 は, 手術不能局所進行性または転移性乳癌に対する臨床試験に使用されており, LDE225 は, 基底細胞癌や, 再発・難治性髄芽腫に対する臨床試験に使用されているため, 今後, 神経膠芽腫への臨床応用が期待される薬剤である.

まとめ

Akt を標的とする分子標的療薬が開発され, 多くの悪性腫瘍の治療薬として, 認容性が良好な治療薬が登場し, 臨床応用されるようになってきており, 神経膠芽腫への応用が期待される. 一方で, 神経膠芽腫は, 複雑で多様なシグナル伝達経路を有し, 単剤投与の限界も確認されてきているのが現状である. 神経膠芽腫に対する治療成績向上のためには, 複数のシグナル伝達経路を抑制する多剤併用分子標的療法の効果を検証する preclinical study が重要であると考えられる.

謝辞

執筆の機会を与您いただきました前琉球医学会長上里 博先生に謝意を表します.

REFERENCES

1) Maher EA, Furnari FB, Bachoo RM, et al.

- Malignant glioma: genetics and biology of a grave matter. *Genes Dev.* 15:1311-1333, 2001.
- 2) Stupp R, Mason WP, van den Bent MJ, et al. Radiotherapy plus concomitant and adjuvant temozolomide for glioblastoma. *N Engl J Med.* 352:987-996, 2005.
- 3) Wen PY, Kesari S. Malignant gliomas in adults. *N Engl J Med.* 359:492-507, 2008.
- 4) Hegi ME, Diserens AC, Gorlia T, et al. MGMT gene silencing and benefit from temozolomide in glioblastoma. *N Engl J Med.* 352:997-1003, 2005.
- 5) Natsume A, Ishii D, Wakabayashi T, et al. IFN-beta down-regulates the expression of DNA repair gene MGMT and sensitizes resistant glioma cells to temozolomide. *Cancer Res.* 65:7573-7579, 2005.
- 6) Wakabayashi T, Kayama T, Nishikawa R, et al. A multicenter phase I trial of combination therapy with interferon-beta and temozolomide for high-grade gliomas (INTEGRA study): the final report. *J Neurooncol.* 104:573-577, 2011.
- 7) Chinot OL, Wick W, Mason W, et al. Bevacizumab plus radiotherapy-temozolomide for newly diagnosed glioblastoma. *N Engl J Med.* 370:709-722, 2014.
- 8) Gilbert MR, Dignam JJ, Armstrong TS, et al. A randomized trial of bevacizumab for newly diagnosed glioblastoma. *N Engl J Med.* 370:699-708, 2014.
- 9) Ishiuchi S, Yoshida Y, Sugawara K, et al. Ca²⁺-permeable AMPA receptors regulate growth of human glioblastoma via Akt activation. *J Neurosci.* 27:7987-8001, 2007.
- 10) Choe G, Horvath S, Cloughesy TF, et al. Analysis of the phosphatidylinositol 3'-kinase signaling pathway in glioblastoma patients in vivo. *Cancer Res.* 63:2742-2746, 2003.
- 11) Datta SR, Brunet A, Greenberg ME. Cellular survival: a play in three Akts. *Genes Dev.* 13:2905-2927, 1999.
- 12) Datta SR, Dudek H, Tao X, et al. Akt phosphorylation of BAD couples survival signals to the cell-intrinsic death machinery. *Cell.* 91:231-241, 1997.
- 13) Holland EC. Gliomagenesis: genetic alterations and mouse models. *Nat Rev Genet.* 2:120-129, 2001.
- 14) Holland EC, Celestino J, Dai C, Schaefer L, Sawaya RE, Fuller GN. Combined activation of

- Ras and Akt in neural progenitors induces glioblastoma formation in mice. *Nat Genet.* 25:55-57, 2000.
- 15) Bochet P, Audinat E, Lambolez B, et al. Subunit composition at the single-cell level explains functional properties of a glutamate-gated channel. *Neuron.* 12:383-388, 1994.
 - 16) Cully M, You H, Levine AJ, Mak TW. Beyond PTEN mutations: the PI3K pathway as an integrator of multiple inputs during tumorigenesis. *Nat Rev Cancer.* 6:184-192, 2006.
 - 17) Engelman JA, Luo J, Cantley LC. The evolution of phosphatidylinositol 3-kinases as regulators of growth and metabolism. *Nat Rev Genet.* 7:606-619, 2006.
 - 18) Alessi DR, Cohen P. Mechanism of activation and function of protein kinase B. *Curr Opin Genet Dev.* 8:55-62, 1998.
 - 19) Williams MR, Arthur JS, Balendran A, et al. The role of 3-phosphoinositide-dependent protein kinase 1 in activating AGC kinases defined in embryonic stem cells. *Curr Biol.* 10:439-448, 2000.
 - 20) Maehama T, Dixon JE. The tumor suppressor, PTEN/MMAC1, dephosphorylates the lipid second messenger, phosphatidylinositol 3,4,5-trisphosphate. *J Biol Chem.* 273:13375-13378, 1998.
 - 21) Blume-Jensen P, Hunter T. Oncogenic kinase signalling. *Nature.* 411:355-365, 2001.
 - 22) Joensuu H, Pupa M, Sihto H, Tynninen O, Nupponen NN. Amplification of genes encoding KIT, PDGFRalpha and VEGFR2 receptor tyrosine kinases is frequent in glioblastoma multiforme. *J Pathol* 207:224-231, 2005.
 - 23) Hermanson M, Funai K, Hartman M, et al. Platelet-derived growth factor and its receptors in human glioma tissue: expression of messenger RNA and protein suggests the presence of autocrine and paracrine loops. *Cancer Res.* 52:3213-3219, 1992.
 - 24) Guha A, Dashner K, Black PM, Wagner JA, Stiles CD. Expression of PDGF and PDGF receptors in human astrocytoma operation specimens supports the existence of an autocrine loop. *Int J Cancer* 60:168-173, 1995.
 - 25) Lokker NA, Sullivan CM, Hollenbach SJ, Israel MA, Giese NA. Platelet-derived growth factor (PDGF) autocrine signaling regulates survival and mitogenic pathways in glioblastoma cells: evidence that the novel PDGF-C and PDGF-D ligands may play a role in the development of brain tumors. *Cancer Res.* 62:3729-3735, 2002.
 - 26) Berdel WE, de Vos S, Maurer J, et al. Recombinant human stem cell factor stimulates growth of a human glioblastoma cell line expressing c-kit protooncogene. *Cancer Res.* 52:3498-3502, 1992.
 - 27) Jansen M, de Witt Hamer PC, Witmer AN, Troost D, van Noorden CJ. Current perspectives on antiangiogenesis strategies in the treatment of malignant gliomas. *Brain research Brain research reviews.* 45:143-163, 2004.
 - 28) Seeburg PH, Osten P. Neurobiology: a thorny issue. *Nature.* 424:627-628, 2003.
 - 29) Yoshida Y, Tsuzuki K, Ishiuchi S, Ozawa S. Serum-dependence of AMPA receptor-mediated proliferation in glioma cells. *Pathol Int.* 56:262-271, 2006.
 - 30) Ishiuchi S, Tsuzuki K, Yoshida Y, et al. Blockage of Ca(2+)-permeable AMPA receptors suppresses migration and induces apoptosis in human glioblastoma cells. *Nat Med.* 8:971-978, 2002.
 - 31) Gruber Filbin M, Dabral SK, Pazyra-Murphy MF, et al. Coordinate activation of Shh and PI3K signaling in PTEN-deficient glioblastoma: new therapeutic opportunities. *Nat Med.* 19:1518-1523, 2013.
 - 32) Stommel JM, Kimmelman AC, Ying H, et al. Coactivation of receptor tyrosine kinases affects the response of tumor cells to targeted therapies. *Science.* 318:287-290, 2007.
 - 33) Shimizu-Sasamata M, Kano T, Rogowska J, Wolf GL, Moskowitz MA, Lo EH. YM872, a highly water-soluble AMPA receptor antagonist, preserves the hemodynamic penumbra and reduces brain injury after permanent focal ischemia in rats. *Stroke.* 29:2141-2148, 1998.
 - 34) Howes JF, Bell C. Talampanel. *Neurotherapeutics.* 4:126-129, 2007.
 - 35) Grossman SA, Ye X, Chamberlain M, et al. Talampanel with standard radiation and temozolomide in patients with newly diagnosed glioblastoma: a multicenter phase II trial. *J Clin Oncol.* 27:4155-4161, 2009.
 - 36) Iwamoto FM, Kreisl TN, Kim L, et al. Phase 2 trial of talampanel, a glutamate receptor

- inhibitor, for adults with recurrent malignant gliomas. *Cancer*. 116:1776-1782, 2010.
- 37) Savage DG, Antman KH. Imatinib mesylate--a new oral targeted therapy. *N Engl J Med*. 346:683-693, 2002.
- 38) Druker BJ, Guilhot F, O'Brien SG, et al. Five-year follow-up of patients receiving imatinib for chronic myeloid leukemia. *N Engl J Med*. 355:2408-2417, 2006.
- 39) Druker BJ, Talpaz M, Resta DJ, et al. Efficacy and safety of a specific inhibitor of the BCR-ABL tyrosine kinase in chronic myeloid leukemia. *N Engl J Med*. 344:1031-1037, 2001.
- 40) Wen PY, Yung WK, Lamborn KR, et al. Phase I/II study of imatinib mesylate for recurrent malignant gliomas: North American Brain Tumor Consortium Study 99-08. *Clin Cancer Res*. 12:4899-4907, 2006.
- 41) Friedman HS, Prados MD, Wen PY, et al. Bevacizumab alone and in combination with irinotecan in recurrent glioblastoma. *J Clin Oncol*. 27:4733-4740, 2009.
- 42) Nagane M, Nishikawa R, Narita Y, et al. Phase II study of single-agent bevacizumab in Japanese patients with recurrent malignant glioma. *Japanese journal of clinical oncology*. 42:887-895, 2012.
- 43) Raizer JJ, Grimm S, Chamberlain MC, et al. A phase 2 trial of single-agent bevacizumab given in an every-3-week schedule for patients with recurrent high-grade gliomas. *Cancer*. 116:5297-5305, 2010.
- 44) Watanabe T, Ohtani T, Aihara M, Ishiuchi S. Enhanced antitumor effect of YM872 and AG1296 combination treatment on human glioblastoma xenograft models. *Journal of neurosurgery* 118:838-845, 2013.